Binned multinomial logistic regression for integrative cell type annotation

Keshav Motwani[1], Rhonda Bacher[2,3], and Aaron J. Molstad[1,3*]
Department of Statistics[1], Department of Biostatistics[2],
and Genetics Institute[3], University of Florida

Abstract

Categorizing individual cells into one of many known cell type categories, also known as cell type annotation, is a critical step in the analysis of single-cell genomics data. The current process of annotation is time-intensive and subjective, which has led to different studies describing cell types with labels of varying degrees of resolution. While supervised learning approaches have provided automated solutions to annotation, there remains a significant challenge in fitting a unified model for multiple datasets with inconsistent labels. In this article, we propose a new multinomial logistic regression estimator which can be used to model cell type probabilities by integrating multiple datasets with labels of varying resolution. To compute our estimator, we solve a nonconvex optimization problem using a blockwise proximal gradient descent algorithm. We show through simulation studies that our approach estimates cell type probabilities more accurately than competitors in a wide variety of scenarios. We apply our method to ten single-cell RNA-seq datasets and demonstrate its utility in predicting fine resolution cell type labels on unlabeled data as well as refining cell type labels on data with existing coarse resolution annotations. An R package implementing the method is available at `https://github.com/keshav-motwani/IBMR` and the collection of datasets we analyze is available at `https://github.com/keshav-motwani/AnnotatedPBMC`.

Keywords: Integrative analysis, multinomial logistic regression, variable selection, group lasso, nonconvex optimization, single-cell genomics

1 Introduction

1.1 Overview

One of the first and most important tasks in the analysis of single-cell data is cell type annotation, where individual cells are categorized into one of many known cell type categories

*Correspondence: amolstad@ufl.edu

having well-characterized biological functions. The vast majority of studies perform annotation by first clustering cells based on their gene expression and then manually labeling the clusters based on upregulated marker genes within each cluster (Schaum et al., 2018). This is often time-intensive and arguably subjective, as the set of cell type labels used is inconsistent across studies: they vary based on scientific interests of the investigators, aims of the study, and availability of external data. In turn, a large number of automated methods have been developed to standardize the cell type annotation process, for example, see Table 1 of Pasquini et al. (2021) and references therein.

The vast majority of the existing approaches for automated cell type annotation fit a classification model using a single training dataset (e.g., a dataset collected and annotated by a single investigator/lab), treating normalized gene expression as predictors. Cell types in a new (unannotated) dataset are then predicted according to the fitted model. In Abdelaal et al. (2019), more than 20 such methods were benchmarked and shown to perform well in a variety of settings. However, these methods tended to perform poorly in terms of prediction across datasets (varying by batch, lab, or protocols) and in datasets with a large number of labels (i.e., high resolution cell type categories) (Abdelaal et al., 2019). Furthermore, a crucial choice for these methods is deciding which dataset should be used to train the model. Datasets can differ in numerous ways, but most relevant to the task we consider: they can have drastically different cell type labels and differ in the amount of detail provided by each label across datasets (Ma et al., 2021). The existing annotation approaches are also limited to single training datasets or multiple datasets with consistent cell type labels. Here, we propose a novel approach for automated annotation that overcomes these limitations.

We begin by depicting the situation of differing degrees of resolution in labels used to annotate different datasets in Figure 1. In this hypothetical situation, one has access to three datasets, Datasets 1, 2, and 3, each of which has been expertly annotated manually. In Dataset 1, cells are labeled as either CD4+ or CD8+. If one trained a model using only Dataset 1, the only possible predicted labels for a new dataset would be CD4+ or CD8+. In Dataset 2, the cells are labeled as one of naive CD4+, effector memory CD4+, central memory CD4+, or CD8+, so if one instead trained the model using Dataset 2, it would be possible to predict/annotate the subcategories of CD4+ T-cells with finer resolution labels when compared to Dataset 1. Dataset 3 has finer resolution labels for subcategories of CD8+ cells than Dataset 2, but does not distinguish between the two finer CD4+ memory cell types like Dataset 2. Thus, using a single dataset to train annotation models presents a trade-off between fine resolution labels for subcategories of CD4+ and subcategories of CD8+ cells.

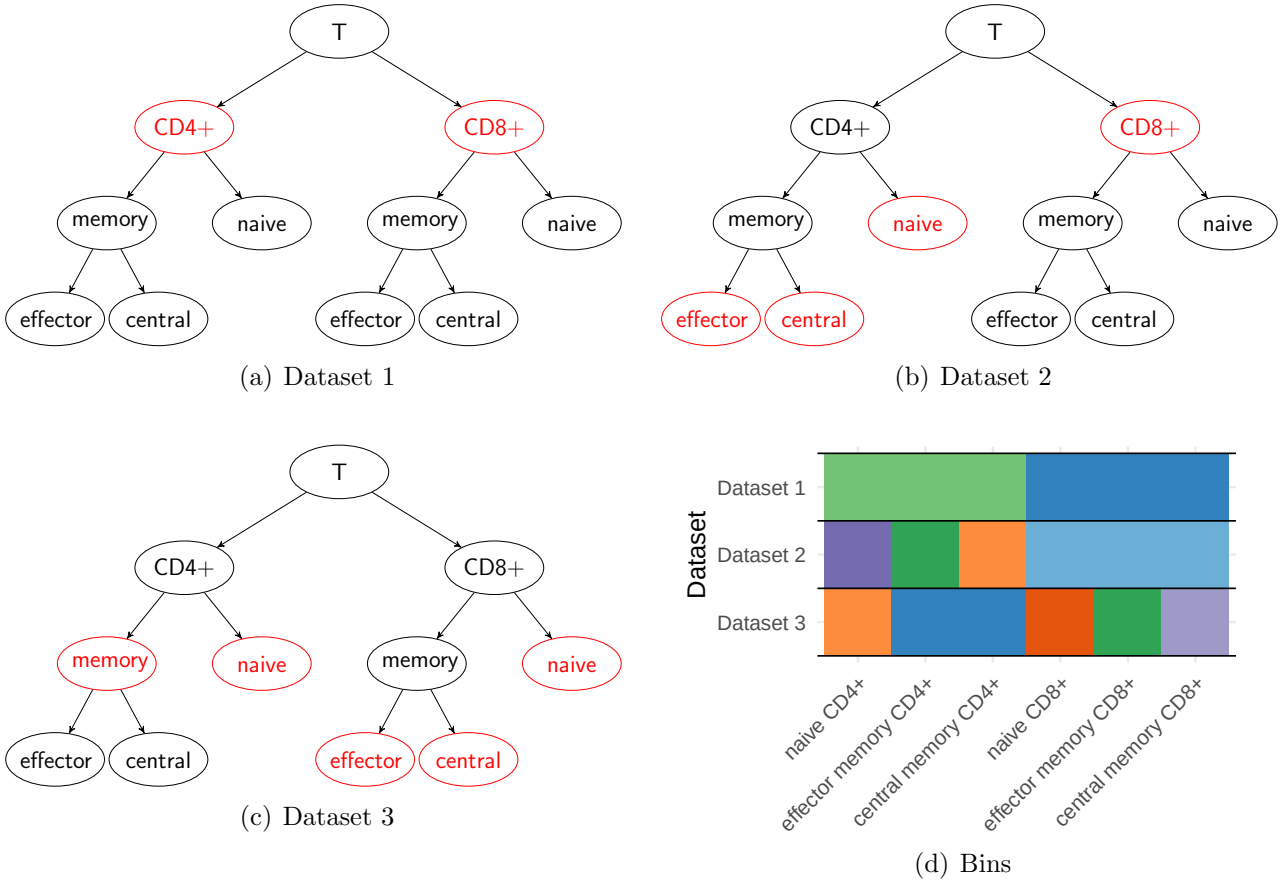

(a) Dataset 1 (b) Dataset 2

(c) Dataset 3 (d) Bins

Figure 1: Illustrative example of label structure across datasets. (a-c) The tree depicts the true hierarchical structure of cell type categories, with cells in Datasets 1–3 annotated at different resolution labels, highlighted in red. Finest resolution categories are defined by the labels at the terminal nodes of the tree. (d) Graphical representation of binning functions for Datasets 1–3 (see Section 2.1), where within each row, a unique color represents a label in that dataset which is a bin of finest resolution categories.

If one wanted to incorporate all datasets into the framework of existing annotation methods, the level of detail in the annotations of Dataset 2 and Dataset 3 must be reduced by labeling cells of all three datasets as one of CD4+ or CD8+. However, this results in a significant loss of information and may limit downstream scientific applications. Alternatively, one could mix-and-match subsets of cells from different datasets which have the most detail for specific cell types. In this example, it would mean taking the subcategories of CD4+ cells from Dataset 2 and subcategories of CD8+ cells from Dataset 3 and ignoring Dataset 1. As such, this approach would be less efficient than one which uses all available data, and moreover, will generalize poorly since technical differences across datasets (i.e., "batch effects")

may be confounded with some cell type categories. Despite the existence of hundreds of publicly available datasets with expertly annotated cell types, existing methods are limited in their ability to integrate a wide-array of datasets due to varying label resolution.

Ideally, we would like to use all the data from all three datasets to train an annotation model without any loss of information. To do so, our proposed approach takes advantage of the "binned" label structures (Figure 1d). For example, cells with the label CD4+ in Dataset 1, biologically, must belong to one of the following finest resolution categories: naive CD4+, effector memory CD4+, or central memory CD4+ The specific label, however, is unknown without additional analysis or manual annotation. In this article, we propose a new classification method which will allow investigators to (i) use all available datasets jointly to train a unified classification model without loss of information, and (ii) make cell type predictions/annotations at the finest resolution labels allowed by the union of all datasets' labels. For example, given the datasets depicted in Figure 1, our method would fit a model using data from all cells from all three datasets, and would yield predicted probabilities of each cell belonging to the categories: naive CD4+, effector memory CD4+, central memory CD4+, naive CD8+, effector memory CD8+, or central memory CD8+ (i.e., the categories at the terminal nodes of the tree). Notably, our method does not require that labels are tree-structured as in this example. We require only that labels are amenable to "binning", which we describe in Section 2.1.

1.2 Existing approaches

The issue of varying labels across datasets has been recognized in the recent single-cell literature. For example, Shasha et al. (2021) manually reannotated publicly available datasets which collected both single-cell gene expression and protein expression data, and fit a cell type classification model across all datasets using reannotated labels with extreme gradient boosting (XGBoost). To reannotate the data, they cleverly employed methods from the field of flow cytometry to "gate" cells based on protein expression using a series of bivariate protein expression plots and manually drawing shapes around groups of cells. This reannotation process, however, is very time-intensive and requires concurrent protein expression in cells. Even with this detailed approach, differences in protein measurements across datasets limited their ability to achieve consistently fine annotations across all datasets. Similarly, Conde et al. (2021) employed a two-step reannotation process. First, with expert input, they attempted to reconcile and rename labels across datasets to achieve a consistent set of labels. Second, they fit a ridge-penalized multinomial logistic regression model on datasets

Dataset	# of labels	Reference(s)
`hao_2020`	28	Hao et al. (2020)
`tsang_2021`	18	Liu et al. (2021)
`haniffa_2021`	16	Stephenson et al. (2021)
`su_2020`	13	Su et al. (2020), Shasha et al. (2021)
`10x_pbmc_5k_v3`	12	10x Genomics (2019), Shasha et al. (2021)
`blish_2020`	12	Wilk et al. (2020)
`kotliarov_2020`	9	Kotliarov et al. (2020)
`10x_pbmc_10k`	9	10x Genomics (2018), Shasha et al. (2021)
`10x_sorted`	8	Zheng et al. (2017)
`ding_2019`	8	Ding et al. (2019)

Table 1: Number of labels and reference(s) for each of the peripheral blood single-cell genomics datasets analyzed in Section 6.

for which they successfully renamed labels for, and used this model to predict the labels for the remaining unresolved datasets. Cells were clustered in each remaining dataset based on gene expression, and each cluster was labeled on a majority vote of the predictions for cells in that cluster. The predicted cluster labels were then treated as true labels for these datasets, and the model was refit using all of the datasets. This approach motivates a two-step approximation to our proposed method, which we term `relabel` (see Section 5.2) and compare to throughout this paper.

1.3 Motivating application

Our motivation for this work was to build a new and generalizable model for high-resolution cell type annotations for peripheral blood mononuclear cell (PBMC) samples by combining many publicly available datasets. We collected and processed a total of ten datasets sequenced using 10x Genomics technology, each with raw gene expression counts and curated cell type annotations available for each cell. We chose to work with PBMC data due to the complexity and hierarchy of immune cell types, as well as the common application of single-cell sequencing of PBMCs in clinical studies (Su et al., 2020; Stephenson et al., 2021; Wilk et al., 2020). Each of the ten datasets have labels at different resolutions, and although labels do not follow a tree-structure across datasets, they are amenable to binning. The number of distinct labels in each dataset, as well as references for the dataset, are shown in Table 1. The specific labels for each dataset are in Table 3 of the Supplementary Material. We display the relationships between labels represented in each of these datasets in

Figure 2 as graphical representations of "binning functions," which are further described in Section 2.1. The datasets we use are available through the R package `AnnotatedPBMC` at `https://github.com/keshav-motwani/AnnotatedPBMC/`, where we also provide an interface to our fitted model for predicting cell types from new single-cell gene expression data.

2 Model

Suppose we observe $K \geq 1$ datasets with single-cell gene expression profiles and cell types manually annotated. Let $\mathcal{C}_k$ denote the set of labels used to annotate the kth dataset for $k \in [K] = \{1, \ldots, K\}$ and let $\mathcal{C}$ denote the set of labels at the desired finest resolution across all datasets. Let $Y_{(k)i}$ and $\tilde{Y}_{(k)i}$ be the random variables corresponding to the annotated cell type and true (according to the finest resolution label set) cell type of the ith cell in the kth dataset for $i \in [n_k] = \{1, \ldots, n_k\}$, $k \in [K]$, with supports $\mathcal{C}_k$ and $\mathcal{C}$, respectively. For the remainder, let $|\mathcal{A}|$ denote the cardinality of a set $\mathcal{A}$. Let $\boldsymbol{X}_{(k)} = (\boldsymbol{x}_{(k)1}, \ldots, \boldsymbol{x}_{(k)n_k})^\top \in \mathbb{R}^{n_k \times p}$ be the observed gene expression matrix, and $(y_{(k)1}, \ldots, y_{(k)n_k})^\top \in \mathcal{C}_k^{n_k}$ be a vector of cell type annotations for the kth dataset where $y_{(k)i}$ is the observed realization of the random variable $Y_{(k)i}$. Similarly, let $\tilde{\boldsymbol{X}}_{(k)} = (\tilde{\boldsymbol{x}}_{(k)1}, \ldots, \tilde{\boldsymbol{x}}_{(k)n_k})^\top \in \mathbb{R}^{n_k \times p}$ for $k \in [K]$ be the unobservable gene expression matrix which is free of batch effects. Our goal is to estimate probabilities $P(\tilde{Y} = l | \boldsymbol{x})$ for $l \in \mathcal{C}$ and any $\boldsymbol{x} \in \mathbb{R}^p$.

2.1 Binned categorical responses

As described earlier, each dataset may have a different degree of resolution in their cell type annotations. Again taking an informal example, we may have two datasets with observed cell type labels in $\mathcal{C}_1 = \{A, B_1, B_2, B_3\}$ for the first dataset and $\mathcal{C}_2 = \{A_1, A_2, B\}$ for the second dataset, with $\mathcal{C} = \{A_1, A_2, B_1, B_2, B_3\}$ being the set of finest categories at which resolution we want to make predictions. We refer to the labels A and B as "coarse labels" since groups of cells with these labels can each be partitioned into finer, more detailed categories (cells with label A can be further divided into categories A_1 or A_2 and cells with label B can be further divided into categories B_1, B_2, or B_3), and refer to each of $\{A_1, A_2, B_1, B_2, B_3\}$ as "fine labels" since they cannot be divided any further into more detailed categories. We refer to data observed at the level of a coarse label as a binned observation, because labels from finer categories are binned into one coarser label. For example, cells that are truly of

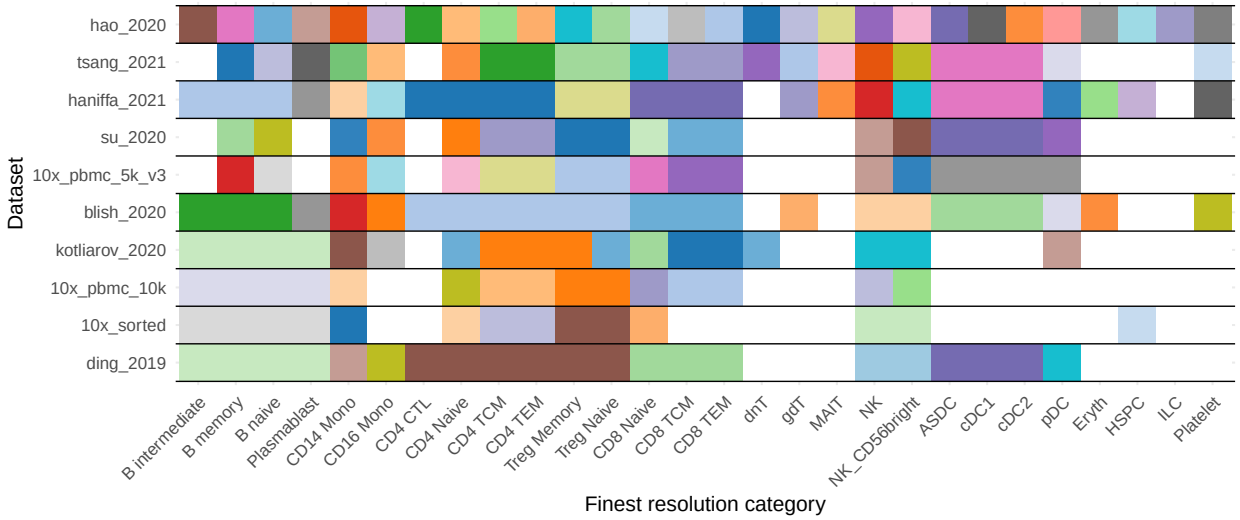

Figure 2: Graphical representation of the relationship between observed (annotated) labels and the finest resolution categories for each of the ten datasets from our integrative analysis in Section 6. Within each row, when a color spans multiple finest resolution categories (columns), this indicates cells of these fine resolution categories were "binned" into a broader annotation label (coarse category) represented by the color. For example, in the `ding_2019` dataset (bottom row), each cell was annotated with one of eight distinct labels. One of these labels was "B cell" (represented by a pastel green color), and cells which could be described in detail as one of either "B intermediate", "B memory," "B naive," or "Plasmablast" are binned into the coarser "B cell" label. White spaces denote finest resolution categories which were not represented by the observed labels in a particular dataset.

cell type A_1 and A_2 are both binned into a label called A in the first dataset. We will now make these ideas and definitions more formal by setting up some additional notation.

Define the user-specified binning function $f_k : \mathcal{C} \to \mathcal{C}_k$ which maps a finest resolution category to the label used to describe that category in the kth dataset. For example, $f_1(A_1) = A$ for dataset 1 above. This function bins fine categories together into the possibly coarser resolution labels which are used in annotating the data, hence the name. Also, define the "unbinning" function $g_k = f_k^{-1}$ (inverse image) where $g_k(j) = f_k^{-1}(j) = \{l \in \mathcal{C} : f_k(l) = j\}$ for $j \in \mathcal{C}_k$. This provides the set of fine categories to which a cell labeled at a coarser resolution category may be further categorized as. For fine categories that are truly not represented in a given dataset, f_k can map from these categories to another label (named "unobserved" for example). While $\mathcal{C}$ and the binning functions f_k are user-specified, they must satisfy the condition that for all $l \in \mathcal{C}$, there must exist $k \in [K]$ and $j \in \mathcal{C}_k$ such that $f_k^{-1}(j) = g_k(j) = \{l\}$ with $\sum_{i=1}^{n_k} \mathbb{1}(y_{(k)i} = j) \geq 1$. In other words, each of the finest resolution

categories must actually be observed at least once in at least one of the K training datasets.

Using this notation, we can now formally define $j \in \mathcal{C}_k$ to be a "coarse label" if $|g_k(j)| > 1$ (i.e., the label can be broken up into multiple finer resolution categories) and a "fine label" if $|g_k(j)| = 1$ (i.e., the label cannot be further partitioned). We also now define the relationship between $Y_{(k)i}$ and $\tilde{Y}_{(k)i}$ through the following equivalence of events

$$\{Y_{(k)i} = j\} = \bigcup_{l \in g_k(j)} \{\tilde{Y}_{(k)i} = l\}, \quad j \in \mathcal{C}_k.$$

That is, a cell can be categorized within one of the finest resolution categories in the bin corresponding to the observed label, with the correspondence defined by g_k. We thus have that

$$P(Y_{(k)i} = j \mid \boldsymbol{x}_{(k)i}) = \sum_{l \in g_k(j)} P(\tilde{Y}_{(k)i} = l \mid \boldsymbol{x}_{(k)i}), \quad j \in \mathcal{C}_k \tag{1}$$

since the events $\{\tilde{Y}_{(k)i} = l : l \in g_k(j)\}$ are mutually exclusive as a cell can only be of one cell type.

2.2 Binned multinomial regression model

As mentioned, we are interested in modeling cell type probabilities as a function of gene expression. For now, we consider a model using unobserved gene expression $\tilde{\boldsymbol{x}}_{(k)i}$, which is free of batch effects, and will extend this in the next section to the observed gene expression. Without loss of generality, we encode the sets of labels numerically so that $\mathcal{C} = \{1, \ldots, |\mathcal{C}|\}$ and $\mathcal{C}_k = \{1, \ldots, |\mathcal{C}_k|\}$ for $k \in [K]$. We assume that each $\tilde{Y}_{(k)i}$ follows a categorical distribution (i.e., multinomial based on a single trial)

$$\tilde{Y}_{(k)i} \sim \text{Categorical}\{\pi^*_1(\tilde{\boldsymbol{x}}_{(k)i}), \ldots, \pi^*_{|\mathcal{C}|}(\tilde{\boldsymbol{x}}_{(k)i})\}.$$

In addition, we assume that the probability functions π^*_l adhere to the standard multinomial logistic regression link so that

$$\pi^*_l(\tilde{\boldsymbol{x}}_{(k)i}) = \frac{\exp(\boldsymbol{\alpha}^*_l + \tilde{\boldsymbol{x}}^\top_{(k)i}\boldsymbol{\beta}^*_l)}{\sum_{v \in \mathcal{C}} \exp(\boldsymbol{\alpha}^*_v + \tilde{\boldsymbol{x}}^\top_{(k)i}\boldsymbol{\beta}^*_v)}, \quad l \in \mathcal{C}, \quad k \in [K],$$

where $\boldsymbol{\alpha}^* = (\boldsymbol{\alpha}^*_1, \ldots, \boldsymbol{\alpha}^*_{|\mathcal{C}|})^\top \in \mathbb{R}^{|\mathcal{C}|}$ is an unknown vector of intercepts and $\boldsymbol{\beta}^* = (\boldsymbol{\beta}^*_1, \ldots, \boldsymbol{\beta}^*_{|\mathcal{C}|}) \in \mathbb{R}^{p \times |\mathcal{C}|}$ is an unknown matrix of regression coefficients. Applying exactly the logic from (1),

it follows that

$$P(Y_{(k)i} = j \mid \tilde{\boldsymbol{x}}_{(k)i}) = \sum_{l \in g_k(j)} \pi_l^*(\tilde{\boldsymbol{x}}_{(k)i}) = \frac{\sum_{l \in g_k(j)} \exp(\boldsymbol{\alpha}_l^* + \tilde{\boldsymbol{x}}_{(k)i}^\top \boldsymbol{\beta}_l^*)}{\sum_{v \in \mathcal{C}} \exp(\boldsymbol{\alpha}_v^* + \tilde{\boldsymbol{x}}_{(k)i}^\top \boldsymbol{\beta}_v^*)}, \quad j \in \mathcal{C}_k, \quad k \in [K].$$

Thus, our focus is the development of a method for estimating $\boldsymbol{\alpha}^*$ and $\boldsymbol{\beta}^*$. However, we first extend the model to account for potential batch effects in the observed gene expression.

2.3 Adjustment for batch effects

The gene expression $\boldsymbol{x}_{(k)i}$ can be assumed to be "noisy" in the sense that they may be measured with some batch effects specific to each of the K datasets. For example, it may be reasonable to assume that $\boldsymbol{x}_{(k)i} = \tilde{\boldsymbol{x}}_{(k)i} + \boldsymbol{u}_{(k)i}$ where $\tilde{\boldsymbol{x}}_{(k)i}$ is the the unobserveable gene expression and $\boldsymbol{u}_{(k)i}$ is some noise. This additive assumption of batch effects is consistent with the existing literature on data integration for normalized gene expression data in single-cell datasets, which provide methods for estimating the $\boldsymbol{u}_{(k)i}$ (Haghverdi et al., 2018; Hao et al., 2020). However, estimating the per-gene batch effect is not necessary for classification: we need only estimate a linear combination of this batch effect, as we now describe.

We can write the linear predictor for the ith cell of the kth dataset as $\boldsymbol{\alpha}^* + \tilde{\boldsymbol{x}}_{(k)i}^\top \boldsymbol{\beta}_l^* = \boldsymbol{\alpha}^* + \boldsymbol{x}_{(k)i}^\top \boldsymbol{\beta}^* - \boldsymbol{u}_{(k)i}^\top \boldsymbol{\beta}^*$. Because the $\boldsymbol{u}_{(k)i}$ are not observable, we assume that there are some common sources of batch variation which are related to some cell-specific covariates $\boldsymbol{z}_{(k)i} \in \mathbb{R}^r$, and that $\boldsymbol{u}_{(k)i}$ is some linear combination of these cell specific covariates $\boldsymbol{u}_{(k)i} = \boldsymbol{z}_{(k)i}^\top \boldsymbol{\phi}_{(k)}^*$ for $i \in [n_k]$, $k \in [K]$, and coefficients $\boldsymbol{\phi}_{(k)}^* \in \mathbb{R}^{r \times p}$. It follows that the linear predictor for the ith cell in the kth dataset is $\boldsymbol{\alpha}^* + \tilde{\boldsymbol{x}}_{(k)i}^\top \boldsymbol{\beta}^* = \boldsymbol{\alpha}^* + \boldsymbol{x}_{(k)i}^\top \boldsymbol{\beta}^* - \boldsymbol{z}_{(k)i}^\top \boldsymbol{\phi}_{(k)}^* \boldsymbol{\beta}^*$ where $\boldsymbol{\alpha}^*$, $\boldsymbol{\beta}^*$, and the $\boldsymbol{\phi}_{(k)}^*$ are unknown. Letting $\boldsymbol{\gamma}_{(k)}^* = -\boldsymbol{\phi}_{(k)}^* \boldsymbol{\beta}^*$ (since both are unknown), we can see that $\boldsymbol{\alpha}^* + \tilde{\boldsymbol{x}}_{(k)i}^\top \boldsymbol{\beta}^* = \boldsymbol{\alpha}^* + \boldsymbol{x}_{(k)i}^\top \boldsymbol{\beta}^* + \boldsymbol{z}_{(k)i}^\top \boldsymbol{\gamma}_{(k)}^*$. Thus, we can write

$$P(Y_{(k)i} = j \mid \boldsymbol{x}_{(k)i}, \boldsymbol{z}_{(k)i}) = \sum_{l \in g_k(j)} \frac{\exp(\boldsymbol{\alpha}_l^* + \boldsymbol{x}_{(k)i}^\top \boldsymbol{\beta}_l^* + \boldsymbol{z}_{(k)i}^\top \boldsymbol{\gamma}_{(k)l}^*)}{\sum_{v \in \mathcal{C}} \exp(\boldsymbol{\alpha}_v^* + \boldsymbol{x}_{(k)i}^\top \boldsymbol{\beta}_v^* + \boldsymbol{z}_{(k)i}^\top \boldsymbol{\gamma}_{(k)v}^*)}, \quad j \in \mathcal{C}_k, \quad k \in [K] \tag{2}$$

In the simplest case, $\boldsymbol{z}_{(k)i} = 1$ (i.e., provides an intercept adjustment), which implies a batch-specific shift in expression that is constant for all cells in the batch. Alternatively, $\boldsymbol{z}_{(k)i}$ can also contain the principal components of $(\boldsymbol{X}_{(1)}^\top, \ldots, \boldsymbol{X}_{(K)}^\top)^\top$ to capture interactions of batch with other directions of variation in the data. It is worth emphasizing that here, we have both batch specific coefficients to estimate, $\boldsymbol{\gamma}_{(k)}^*$ for $k \in [K]$, and coefficients shared across batches, $(\boldsymbol{\alpha}^*, \boldsymbol{\beta}^*)$. With this, our goal will be to estimate $\boldsymbol{\alpha}^*$, $\boldsymbol{\beta}^*$, and $\boldsymbol{\gamma}_{(k)}^*$ via penalized

maximum likelihood based on the observed predictors $\boldsymbol{x}_{(k)i}$ for $i \in [n_k]$ and $k \in [K]$.

3 Methodology

3.1 Penalized maximum likelihood estimator

From the probability functions described in Section 2.3, we see that the log-likelihood contribution for the ith cell in the kth dataset can be expressed

$$l_{(k)i}(\boldsymbol{\alpha}, \boldsymbol{\beta}, \boldsymbol{\gamma}_{(k)}) = \sum_{j \in \mathcal{C}_k} \mathbb{1}(y_{(k)i} = j) \log \left(\sum_{l \in g_k(j)} \frac{\exp(\boldsymbol{\alpha}_l + \boldsymbol{x}_{(k)i}^\top \boldsymbol{\beta}_l + \boldsymbol{z}_{(k)i}^\top \boldsymbol{\gamma}_{(k)l})}{\sum_{v \in \mathcal{C}} \exp(\boldsymbol{\alpha}_v + \boldsymbol{x}_{(k)i}^\top \boldsymbol{\beta}_v + \boldsymbol{z}_{(k)i}^\top \boldsymbol{\gamma}_{(k)v})} \right)$$

for $i \in [n_k]$ and $k \in [K]$, where $\mathbb{1}$ denotes the indicator function. We can therefore define the (scaled by $1/N$) negative log-likelihood as

$$\mathcal{L}(\boldsymbol{\alpha}, \boldsymbol{\beta}, \boldsymbol{\gamma}) = -\frac{1}{N} \sum_{k=1}^{K} \sum_{i=1}^{n_k} l_{(k)i}(\boldsymbol{\alpha}, \boldsymbol{\beta}, \boldsymbol{\gamma}_{(k)}),$$

where $N = \sum_{k=1}^{K} n_k$ is the total sample size and $\boldsymbol{\gamma} = (\boldsymbol{\gamma}_{(1)}, \ldots, \boldsymbol{\gamma}_{(K)}) \in \mathbb{R}^{r \times |\mathcal{C}|} \times \cdots \times \mathbb{R}^{r \times |\mathcal{C}|}$. We thus estimate $\boldsymbol{\alpha}^*$ and $\boldsymbol{\beta}^*$, which are the shared across datasets, and $\boldsymbol{\gamma}_{(k)}^* \in \mathbb{R}^{r \times |\mathcal{C}|}$ for datasets $k \in [K]$ jointly using penalized maximum likelihood. For ease of display, let $\mathcal{T} = \mathbb{R}^{|\mathcal{C}|} \times \mathbb{R}^{p \times |\mathcal{C}|} \times \mathbb{R}^{r \times |\mathcal{C}|} \times \cdots \times \mathbb{R}^{r \times |\mathcal{C}|}$ be the space of the unknown parameters $(\boldsymbol{\alpha}^*, \boldsymbol{\beta}^*, \boldsymbol{\gamma}^*)$. Formally, the estimator of $(\boldsymbol{\alpha}^*, \boldsymbol{\beta}^*, \boldsymbol{\gamma}^*)$ we propose is

$$\underset{(\boldsymbol{\alpha}, \boldsymbol{\beta}, \boldsymbol{\gamma}) \in \mathcal{T}}{\arg\min} \left\{ \mathcal{L}(\boldsymbol{\alpha}, \boldsymbol{\beta}, \boldsymbol{\gamma}) + \lambda \sum_{j=1}^{p} \|\boldsymbol{\beta}_{j,:}\|_2 + \frac{\rho}{2} \sum_{k=1}^{K} \|\boldsymbol{\gamma}_{(k)}\|_F^2 \right\}, \tag{3}$$

where $\boldsymbol{\beta}_{j,:} \in \mathbb{R}^{|\mathcal{C}|}$ denotes the jth row of $\boldsymbol{\beta}$ for $\in [p] = \{1, \ldots, p\}$, $\|\cdot\|_2$ denotes the Euclidean norm of a vector, $\|\cdot\|_F$ denotes the Frobenius norm of a matrix, and $(\lambda, \rho) \in (0, \infty) \times (0, \infty)$ are user-specified tuning parameters. We now motivate the choice of penalties based on our application.

Manual single-cell annotation is often performed through the identification of upregulated genes within clusters of cells (Amezquita et al., 2020). For example, to label a cluster of cells as type CD4+ naive, an annotater often identifies a number of particular genes that are overexpressed in that cluster relative to the rest of the cells (Wolf et al., 2018; Hao et al.,

2020). This implies that a relatively small number of genes are necessary to characterize the relationship between cell type probabilities and gene expression. For this reason we use the group lasso type penalty on the rows of the optimization variable $\boldsymbol{\beta}$ (Yuan and Lin, 2006; Obozinski et al., 2011; Simon et al., 2013). For large values of λ, this penalty will encourage estimates of $\boldsymbol{\beta}^*$ which will have rows either entirely equal to zero or entirely nonzero. If the j-th row of $\boldsymbol{\beta}^*$ is zero, the j-th gene is irrelevant for discriminating between cell types. The L_1(vector)-norm penalty (i.e., the lasso penalty), in contrast, would not lead to easily interpreted variable selection since a zero in a particular entry of $\boldsymbol{\beta}^*$ does not alone imply anything about whether the corresponding predictor affects the probabilities.

Regarding the ridge penalty on the $\boldsymbol{\gamma}_{(k)}$: because the $\boldsymbol{\gamma}_{(k)}$ are specific to each of the training sets, we do not have corresponding coefficients for a test data point from a new (i.e., unobserved for training) dataset. Additionally, we expect that the batch effect does not contain information relevant to cell type classification. Therefore, we intuitively want $\boldsymbol{\gamma}_{(k)}$ to be close to the origin, so that on a test data point, we can simply use our estimates $\hat{\boldsymbol{\alpha}}$ and $\hat{\boldsymbol{\beta}}$ from (3) to estimate probabilities with

$$\hat{P}(\tilde{Y} = l \mid \boldsymbol{x}) = \frac{\exp(\hat{\boldsymbol{\alpha}}_l + \boldsymbol{x}^\top \hat{\boldsymbol{\beta}}_l)}{\sum_{v \in \mathcal{C}} \exp(\hat{\boldsymbol{\alpha}}_v + \boldsymbol{x}^\top \hat{\boldsymbol{\beta}}_v)}, \quad l \in \mathcal{C},$$

as if $\tilde{\boldsymbol{x}} = \boldsymbol{x}$. To encourage estimates of the $\boldsymbol{\gamma}^*_{(k)}$ to be small, we add a penalty of the squared Frobenius norm of each $\boldsymbol{\gamma}_{(k)}$. Additional intuition may be gleaned by considering the Bayesian interpretation of ridge regression wherein the coefficients are assumed to follow a mean zero normal distribution.

Importantly, the coefficients we intend to estimate are not, in general, identifiable. This is because with $\mathbf{1}_{|\mathcal{C}|} = (1, \ldots, 1)^\top \in \mathbb{R}^{|\mathcal{C}|}$, for any $(\boldsymbol{\alpha}, \boldsymbol{\beta}, \boldsymbol{\gamma})$, $\mathcal{L}(\boldsymbol{\alpha}, \boldsymbol{\beta}, \boldsymbol{\gamma}_{(1)}, \ldots, \boldsymbol{\gamma}_{(K)}) = \mathcal{L}(\boldsymbol{\alpha} - a \cdot \mathbf{1}^\top_{|\mathcal{C}|}, \boldsymbol{\beta} - \boldsymbol{b}\mathbf{1}^\top_{|\mathcal{C}|}, \boldsymbol{\gamma}_{(1)} - \boldsymbol{d}_1\mathbf{1}^\top_{|\mathcal{C}|}, \ldots, \boldsymbol{\gamma}_{(K)} - \boldsymbol{d}_K\mathbf{1}^\top_{|\mathcal{C}|})$ for any $a \in \mathbb{R}$, $\boldsymbol{b} \in \mathbb{R}^p$, and $\boldsymbol{d}_k \in \mathbb{R}^r$ for $k \in [K]$. However, if we impose the "sum-to-zero" condition that $\boldsymbol{\alpha}^\top \mathbf{1}_{|\mathcal{C}|} = \boldsymbol{\beta}^\top_{1,:}\mathbf{1}_{|\mathcal{C}|} = \cdots = \boldsymbol{\beta}^\top_{p,:}\mathbf{1}_{|\mathcal{C}|} = 0$, and similarly for the rows of the $\boldsymbol{\gamma}_{(k)}$, then this issue may be resolved. It is perhaps surprising that the $\boldsymbol{\gamma}_{(k)} \in \mathbb{R}^{r \times |\mathcal{C}|}$ could be identifiable since $\mathcal{C}_k$ may be distinct from $\mathcal{C}$, but one can see that replacing $\boldsymbol{\gamma}_{(k)}$ with $\boldsymbol{\gamma}'_{(k)}$ will, in general, lead to distinct probabilities (2) unless $\boldsymbol{\gamma}'_{(k)} = \boldsymbol{\gamma}_{(k)} - \boldsymbol{d}_k\mathbf{1}^\top_{|\mathcal{C}|}$. In the Supplementary Material, we discuss the (exceptionally rare) situations where this is not true. Fortunately, both our penalties naturally enforce the sum-to-zero constraints on $\boldsymbol{\beta}$ and the $\boldsymbol{\gamma}_{(k)}$. For example, see the Supplementary Material of Molstad and Rothman (2021) for a proof of this fact.

3.2 Related methods

The approach proposed here is closely related to a growing literature on methods for integrative analyses. We discuss this literature from two perspectives: that of statistical methodology and that of the analysis of multiple single-cell datasets jointly.

From a methodological perspective, there is a growing interest in developing methods for jointly analyzing datasets from heterogeneous sources. Most often, these methods assume distinct data generating models for each source and aim improve efficiency by exploiting similarities across sources (Zhao et al., 2015; Huang et al., 2017; Ventz et al., 2021; Molstad and Patra, 2021). For example, Huang et al. (2017) assumed a similar sparsity pattern for regression coefficients corresponding to separate populations. Similarly, Molstad and Patra (2021) assumed a shared low-dimensional linear combination of predictors explained the outcome in all sources. The focus of our work is different: the sources from which the data were collected are assumed to differ only in their response category label resolution (and, to a lesser degree, may measure predictors with batch effects). Thus, these approaches are, generally speaking, not directly applicable to our setting.

In the context of single-cell data analysis, integrative analyses often focus on the "alignment" of expression datasets in an attempt to remove batch effects for the purposes of clustering and visualization (Haghverdi et al., 2018; Hie et al., 2019; Korsunsky et al., 2019; Hao et al., 2020). As mentioned in the previous section, explicit estimation and removal of batch effects is not necessary for the goal of cell type prediction. In fact, Ma et al. (2021) found that removing batch effects through alignment-based methods actually decreased downstream cell type prediction accuracy. Our inclusion of batch specific effects in (2) can, loosely speaking, be thought of as performing alignment specifically tailored to prediction (assuming the $\boldsymbol{z}_{(k)i}$ are chosen appropriately).

4 Computation

In order to compute our proposed estimator, we must address that the group lasso penalty is nondifferentiable at zero and that the overall negative log-likelihood $\mathcal{L}$ is nonconvex in general. In brief, we employ a blockwise proximal gradient descent scheme (Xu and Yin, 2017) to overcome these challenges. Specifically, we obtain a new iterate by minimizing a penalized quadratic approximation to $\mathcal{L}$ at the current iterate, which will ensure – by the majorize-minimize principle (Lange, 2016) – a monotonically decreasing objective function value. Our approximations are chosen so as to admit simple, closed form updates for each

block. In the remainder of this section, we motivate and derive each block update and summarize our algorithm. Code implementing the algorithm described here is available for download at `https://github.com/keshav-motwani/IBMR/`.

Let $\mathcal{F}_{\lambda,\rho}$ denote the objective function from (3). By construction, $\mathcal{F}_{0,0}$ denotes the negative log-likelihood $\mathcal{L}$. To describe our iterative procedure, we focus on the update for $\boldsymbol{\beta}$, but as we will show, this approach also applies to $\boldsymbol{\alpha}$ and the $\boldsymbol{\gamma}_{(k)}$ with minor modification. First, notice that given t-th iterates of $\boldsymbol{\alpha}, \boldsymbol{\beta}$ and $\boldsymbol{\gamma}$, $(\boldsymbol{\alpha}^t, \boldsymbol{\beta}^t, \boldsymbol{\gamma}^t)$, by the Lipschitz continuity of the gradient of $\mathcal{L}$ when treated as a function of $\boldsymbol{\beta}$ alone, we know that for any step size s_β such that $0 < s_\beta < N/\{\sqrt{|\mathcal{C}|}\sum_{k=1}^K \|\boldsymbol{X}_{(k)}\|_F^2\}$,

$$\mathcal{F}_{0,0}(\boldsymbol{\alpha}^t, \boldsymbol{\beta}, \boldsymbol{\gamma}^t) \leq \mathcal{F}_{0,0}(\boldsymbol{\alpha}^t, \boldsymbol{\beta}^t, \boldsymbol{\gamma}^t) + \operatorname{tr}\left\{\nabla_\beta \mathcal{F}_{0,0}(\boldsymbol{\alpha}^t, \boldsymbol{\beta}^t, \boldsymbol{\gamma}^t)^\top (\boldsymbol{\beta} - \boldsymbol{\beta}^t)\right\} + \frac{1}{2s_\beta}\|\boldsymbol{\beta} - \boldsymbol{\beta}^t\|_F^2$$

for all $\boldsymbol{\beta} \in \mathbb{R}^{p\times|\mathcal{C}|}$, where $\nabla_\beta \mathcal{F}_{0,0}(\boldsymbol{\alpha}^t, \cdot, \boldsymbol{\gamma}^t)$ denotes the gradient of $\boldsymbol{\beta} \mapsto \mathcal{F}_{0,0}(\boldsymbol{\alpha}^t, \boldsymbol{\beta}, \boldsymbol{\gamma}^t)$. Letting $\mathcal{M}(\boldsymbol{\beta} \mid \boldsymbol{\beta}^t)$ denote the right-hand side of the above inequality, we can see that

$$\mathcal{F}_{\lambda,\rho}(\boldsymbol{\alpha}^t, \boldsymbol{\beta}, \boldsymbol{\gamma}^t) \leq \mathcal{M}(\boldsymbol{\beta} \mid \boldsymbol{\beta}^t) + \lambda\sum_{j=1}^p \|\boldsymbol{\beta}_{j,:}\|_2 + \frac{\rho}{2}\sum_{k=1}^K \|\boldsymbol{\gamma}_{(k)}^t\|_F^2,$$

for all $\boldsymbol{\beta} \in \mathbb{R}^{p\times|\mathcal{C}|}$ with equality when $\boldsymbol{\beta} = \boldsymbol{\beta}^t$. If we thus define $\boldsymbol{\beta}^{t+1}$ as the argument minimizing $\mathcal{M}(\boldsymbol{\beta} \mid \boldsymbol{\beta}^t) + \lambda\sum_{j=1}^p \|\boldsymbol{\beta}_{j,:}\|_2$, we are ensured that $\mathcal{F}_{\lambda,\gamma}(\boldsymbol{\alpha}^t, \boldsymbol{\beta}^{t+1}, \boldsymbol{\gamma}^t) \leq \mathcal{F}_{\lambda,\gamma}(\boldsymbol{\alpha}^t, \boldsymbol{\beta}^t, \boldsymbol{\gamma}^t)$. Hence, defining $\boldsymbol{\beta}^{t+1}$ in this way, we have

$$\boldsymbol{\beta}^{t+1} = \operatorname*{arg\,min}_{\boldsymbol{\beta}\in\mathbb{R}^{|\mathcal{C}|}} \left\{\mathcal{M}(\boldsymbol{\beta} \mid \boldsymbol{\beta}^t) + \lambda\sum_{j=1}^p \|\boldsymbol{\beta}_{j,:}\|_2\right\} = \operatorname*{arg\,min}_{\boldsymbol{\beta}\in\mathbb{R}^{|\mathcal{C}|}} \left\{\frac{1}{2}\|\boldsymbol{\beta} - \boldsymbol{\nu}^t(s_\beta)\|_F^2 + s_\beta\lambda\sum_{j=1}^p \|\boldsymbol{\beta}_{j,:}\|_2\right\},$$

where $\boldsymbol{\nu}^t(s_\beta) = \boldsymbol{\beta}^t - s_\beta\nabla_\beta\mathcal{F}_{0,0}(\boldsymbol{\alpha}^t, \boldsymbol{\beta}^t, \boldsymbol{\gamma}^t)$. The second equality above implies that $\boldsymbol{\beta}^{t+1}$ is simply the proximal operator (Parikh and Boyd, 2014; Polson et al., 2015) of the $\|\cdot\|_{1,2}$-norm (sum of Euclidean norm of the rows of its matrix-valued argument) at $\boldsymbol{\nu}^t(s_\beta)$. Some straightforward derivations (e.g., see Simon et al. (2013)) reveal that the jth row of $\boldsymbol{\beta}^{t+1}$, $\boldsymbol{\beta}_{j,:}^{t+1}$, can thus be obtained in closed form

$$\boldsymbol{\beta}_{j,:}^{t+1} = \max\left(1 - \frac{s_\beta\lambda}{\|\boldsymbol{\nu}^t(s_\beta)_{j,:}\|_2}, 0\right)\boldsymbol{\nu}^t(s_\beta)_{j,:}, \quad j \in [p].$$

We apply analogous arguments to update both $\boldsymbol{\gamma}$ with $(\boldsymbol{\alpha}^t, \boldsymbol{\beta}^{t+1})$ fixed and $\boldsymbol{\alpha}$ with $(\boldsymbol{\beta}^{t+1}, \boldsymbol{\gamma}^{t+1})$ fixed. For $\boldsymbol{\alpha}$, yields a standard gradient descent update, whereas for the $\boldsymbol{\gamma}_{(k)}$, each can be

Algorithm 1 Blockwise proximal gradient descent algorithm for minimizing $\mathcal{F}_{\lambda,\rho}$

Initialize $\boldsymbol{\beta}^0 \in \mathbb{R}^{p\times|\mathcal{C}|}$, $\boldsymbol{\alpha}^0 \in \mathbb{R}^{|\mathcal{C}|}$, and $\boldsymbol{\gamma}_{(k)}^0 \in \mathbb{R}^{r\times|\mathcal{C}|}$ for $k \in [K]$. Set $t = 0$.

1. Compute $\boldsymbol{\nu}^t(s_\beta) = \boldsymbol{\beta}^t - s_\beta \nabla_\beta \mathcal{F}_{0,0}(\boldsymbol{\alpha}^t, \boldsymbol{\beta}^t, \boldsymbol{\gamma}^t)$
2. For $j \in [p]$ in parallel, compute

$$\boldsymbol{\beta}_{j,:}^{t+1} = \max\left(1 - \frac{s_\beta \lambda}{\|\boldsymbol{\nu}^t(s_\beta)_{j,:}\|_2}, 0\right) \boldsymbol{\nu}^t(s_\beta)_{j,:}$$

   with s_β chosen by backtracking line search.
3. For $k \in [K]$ in parallel, compute

$$\boldsymbol{\gamma}_{(k)}^{t+1} = \left(1 + s_{\gamma_{(k)}}\rho\right)^{-1} \left\{\boldsymbol{\gamma}_{(k)}^t - s_{\gamma_{(k)}} \nabla_{\boldsymbol{\gamma}_{(k)}} \mathcal{F}_{0,0}(\boldsymbol{\alpha}^t, \boldsymbol{\beta}^{t+1}, \boldsymbol{\gamma}^t)\right\}$$

   with the $s_{\gamma_{(k)}}$ chosen by backtracking line search.
4. Compute $\boldsymbol{\alpha}^{t+1} = \boldsymbol{\alpha}^t - s_\alpha \nabla_{\alpha_{(k)}} \mathcal{F}_{0,0}(\boldsymbol{\alpha}^t, \boldsymbol{\beta}^{t+1}, \boldsymbol{\gamma}^{t+1})$ with s_α chosen by backtracking line search.
5. If objective function value has not converged, set $t = t + 1$ and return to 1.

updated in parallel. Specifically, by the same motivation as in the update for $\boldsymbol{\beta}$, we define

$$\begin{aligned}\boldsymbol{\gamma}_{(k)}^{t+1} &= \underset{\boldsymbol{\gamma}_{(k)}\in\mathbb{R}^{r\times|\mathcal{C}|}}{\arg\min} \left\{\frac{1}{2}\|\boldsymbol{\gamma}_{(k)} - \boldsymbol{\gamma}_{(k)}^t + s_{\gamma_{(k)}} \nabla_{\gamma_{(k)}} \mathcal{F}_{0,0}(\boldsymbol{\alpha}^t, \boldsymbol{\beta}^{t+1}, \boldsymbol{\gamma}^t)\|_F^2 + \frac{s_{\gamma_{(k)}}\rho}{2}\|\boldsymbol{\gamma}_{(k)}\|_F^2\right\} \\ &= \left(1 + s_{\gamma_{(k)}}\rho\right)^{-1} \left\{\boldsymbol{\gamma}_{(k)}^{t+1} - s_{\gamma_{(k)}} \nabla_{\gamma_{(k)}} \mathcal{F}_{0,0}(\boldsymbol{\alpha}^t, \boldsymbol{\beta}^{t+1}, \boldsymbol{\gamma}^t)\right\}.\end{aligned}$$

With these updating expressions for $\boldsymbol{\beta}, \boldsymbol{\alpha}$, and $\boldsymbol{\gamma}$ in hand, we formally state our iterative procedure for minimizing $\mathcal{F}_{\lambda,\rho}$ in Algorithm 1. Applying an identical series of arguments as those to prove that $\boldsymbol{\beta}^{t+1}$ yields a decrement of the objective function, we have the following lemma regarding the sequence of iterates $\{(\boldsymbol{\beta}^t, \boldsymbol{\alpha}^t, \boldsymbol{\gamma}^t)\}_{t=0}^\infty$.

Lemma 1. *(Descent property) As long as each step size $s_\beta > 0, s_\alpha > 0, s_{\gamma_{(k)}} > 0$ is sufficiently small and fixed or chosen by backtracking line search (see the Supplementary Material), the sequence of iterates $\{(\boldsymbol{\beta}^t, \boldsymbol{\alpha}^t, \boldsymbol{\gamma}^t)\}_{t=0}^\infty$ is guaranteed to satisfy $\mathcal{F}_{\lambda,\rho}(\boldsymbol{\alpha}^{t+1}, \boldsymbol{\beta}^{t+1}, \boldsymbol{\gamma}^{t+1}) \leq \mathcal{F}_{\lambda,\rho}(\boldsymbol{\alpha}^t, \boldsymbol{\beta}^t, \boldsymbol{\gamma}^t)$, for $t = 1, 2, 3, \ldots$, i.e., Algorithm 1 has the descent property.*

In the Supplementary Material, we derive explicit forms of the partial derivatives needed in Algorithm 1. Because they provide some insight, we discuss them here. For each $k \in [K]$,

let $\tilde{\boldsymbol{P}}_{(k)} : \mathbb{R}^{|\mathcal{C}|} \times \mathbb{R}^{p\times|\mathcal{C}|} \times \mathbb{R}^{r\times|\mathcal{C}|} \times \cdots \mathbb{R}^{r\times|\mathcal{C}|} \to \mathbb{R}^{n\times|\mathcal{C}|}$ be a matrix-valued function which maps input parameters $(\boldsymbol{\alpha}, \boldsymbol{\beta}, \boldsymbol{\gamma})$ to a matrix of (unconditional) probabilities. Specifically, $\tilde{\boldsymbol{P}}_{(k)}(\boldsymbol{\alpha}, \boldsymbol{\beta}, \boldsymbol{\gamma}_{(k)})$ has (i, l)-th entry

$$[\tilde{\boldsymbol{P}}_{(k)}(\boldsymbol{\alpha}, \boldsymbol{\beta}, \boldsymbol{\gamma}_{(k)})]_{i,l} = \frac{\exp(\boldsymbol{\alpha}_l + \boldsymbol{x}_{(k)i}^\top \boldsymbol{\beta}_l + \boldsymbol{z}_{(k)i}^\top \boldsymbol{\gamma}_{(k)l})}{\sum_{v\in\mathcal{C}} \exp(\boldsymbol{\alpha}_v + \boldsymbol{x}_{(k)i}^\top \boldsymbol{\beta}_v + \boldsymbol{z}_{(k)i}^\top \boldsymbol{\gamma}_{(k)v})}, \quad l \in \mathcal{C}, \quad i \in [n_k], \quad k \in [K]. \tag{4}$$

Similarly, let $\tilde{\boldsymbol{C}}_{(k)} : \mathbb{R}^{|\mathcal{C}|} \times \mathbb{R}^{p\times|\mathcal{C}|} \times \mathbb{R}^{r\times|\mathcal{C}|} \times \cdots \mathbb{R}^{r\times|\mathcal{C}|} \to \mathbb{R}^{n\times|\mathcal{C}|}$ be a matrix-valued function of conditional probabilities where

$$[\tilde{\boldsymbol{C}}_{(k)}(\boldsymbol{\alpha}, \boldsymbol{\beta}, \boldsymbol{\gamma}_{(k)})]_{i,l} = \frac{\mathbb{1}\{l \in g_k(y_{(k)i})\} \exp(\boldsymbol{\alpha}_l + \boldsymbol{x}_{(k)i}^\top \boldsymbol{\beta}_l + \boldsymbol{z}_{(k)i}^\top \boldsymbol{\gamma}_{(k)l})}{\sum_{v\in g_k(y_{(k)i})} \exp(\boldsymbol{\alpha}_v + \boldsymbol{x}_{(k)i}^\top \boldsymbol{\beta}_v + \boldsymbol{z}_{(k)i}^\top \boldsymbol{\gamma}_{(k)v})}, \quad l \in \mathcal{C}, \ i \in [n_k], \ k \in [K]. \tag{5}$$

Intuitively, $[\tilde{\boldsymbol{P}}_{(k)}(\boldsymbol{\alpha}, \boldsymbol{\beta}, \boldsymbol{\gamma}_{(k)})]_{i,l}$ is the estimated probability that cell i from dataset k is of type l. The conditional probability $[\tilde{\boldsymbol{C}}_{(k)}(\boldsymbol{\alpha}, \boldsymbol{\beta}, \boldsymbol{\gamma}_{(k)})]_{i,l}$ is the estimated probability that cell i from dataset k is of type $l \in \mathcal{C}$ given $y_{(k)i}$ is the observed (possibly coarse) label. Of course, if $g_k(y_{(k)i})$ is a singleton, then $[\tilde{\boldsymbol{C}}_{(k)}(\boldsymbol{\alpha}, \boldsymbol{\beta}, \boldsymbol{\gamma}_{(k)})]_{i,l} = \mathbb{1}\{l \in g_k(y_{(k)i})\}$.

The gradients needed in Algorithm 1 can be expressed in terms of $\tilde{\boldsymbol{P}}$ and $\tilde{\boldsymbol{C}}$. In particular,

$$\begin{aligned}
\nabla_\beta \mathcal{F}_{0,0}(\boldsymbol{\alpha}^t, \boldsymbol{\beta}, \boldsymbol{\gamma}^t) &= \frac{1}{N} \sum_{k=1}^K \boldsymbol{X}_{(k)}^\top \left\{ \tilde{\boldsymbol{P}}_{(k)}(\boldsymbol{\alpha}^t, \boldsymbol{\beta}, \boldsymbol{\gamma}_{(k)}^t) - \tilde{\boldsymbol{C}}_{(k)}(\boldsymbol{\alpha}^t, \boldsymbol{\beta}, \boldsymbol{\gamma}_{(k)}^t) \right\}, \\
\nabla_\alpha \mathcal{F}_{0,0}(\boldsymbol{\alpha}, \boldsymbol{\beta}^{t+1}, \boldsymbol{\gamma}^{t+1}) &= \frac{1}{N} \sum_{k=1}^K \left\{ \tilde{\boldsymbol{P}}_{(k)}(\boldsymbol{\alpha}, \boldsymbol{\beta}^{t+1}, \boldsymbol{\gamma}_{(k)}^{t+1}) - \tilde{\boldsymbol{C}}_{(k)}(\boldsymbol{\alpha}, \boldsymbol{\beta}^{t+1}, \boldsymbol{\gamma}_{(k)}^{t+1}) \right\}^\top \mathbf{1}_{n_k}, \\
\nabla_{\gamma_{(k)}} \mathcal{F}_{0,0}(\boldsymbol{\alpha}^t, \boldsymbol{\beta}^{t+1}, \boldsymbol{\gamma}) &= \frac{1}{N} \boldsymbol{Z}_{(k)}^\top \left\{ \tilde{\boldsymbol{P}}_{(k)}(\boldsymbol{\alpha}^t, \boldsymbol{\beta}^{t+1}, \boldsymbol{\gamma}_{(k)}) - \tilde{\boldsymbol{C}}_{(k)}(\boldsymbol{\alpha}^t, \boldsymbol{\beta}^{t+1}, \boldsymbol{\gamma}_{(k)}) \right\}, \quad k \in [K].
\end{aligned}$$

Examining the form of these gradients, loosely speaking, we see our algorithm descends in the direction determined the correlation between the predictors and the difference between the unconditional and conditional estimated probabilities. The functions $\tilde{\boldsymbol{P}}$ and $\tilde{\boldsymbol{C}}$ are also used later when we apply our method to the motivating data analysis.

In the Supplementary Material, we detail how we construct a set of candidate tuning parameters (λ, ρ) yielding sparse fitted models. In brief, we use the KKT condition for (3) to find a λ yielding $\hat{\boldsymbol{\beta}} = \mathbf{0}$ and borrow an approach from `glmnet` for determining a reasonable set of values for ρ.

5 Simulation studies

We performed extensive numerical experiments to study how the sample size, number of predictors, similarity of categories, and the magnitude of batch effects affect the performance of various methods for estimating finest resolution cell type probabilities.

5.1 Data generating models

For each replication, we generated a total of 13 datasets: six datasets with sample size $N/6$ for fitting the model, six datasets with sample size $N/6$ for validation, and one dataset with sample size 10^4 for evaluating performance. We considered $N \in \{2400, 4800, 9600, 19200\}$ to reflect the large number of cells available in real datasets. We set the number of finest resolution categories to be fixed at 12 ($\mathcal{C} = \{A_1, A_2, B_1, B_2, C_1, C_2, D_1, D_2, E_1, E_2, F_1, F_2\}$) and the binning functions fixed to have a structure inspired by the real data as shown by Figure 2. Specifically, in the real data, most cell types are observed at a coarse resolution in most datasets and at finest resolution in only a few datasets. Therefore, we chose to bin categories $A_1, A_2, B_1, B_2, C_1, C_2, D_1, D_2, E_1,$ and E_2 into groups of two for Datasets 1–4. That is categories A_1 and A_2 are binned together, B_1 and B_2 are binned together, and so on. However, we set it so that these categories would be observed at the finest resolution in Datasets 5 and 6. Also, in the real data, some cell types are labeled at the finest resolution in all datasets (for example, CD14+ Monocytes and CD16+ Monocytes in Figure 2). Hence, we chose categories F_1 and F_2 to be observed at the finest resolution in all datasets. A graphical representation of these binning functions is shown in Figure B.1 of the Supplementary Material. The validation datasets, Datasets 7–12, are generated in the same way as Datasets 1–6. For the test dataset, all observations are observed at the finest resolution in order to fully evaluate parameter estimation.

In manual single-cell annotation, cell types are binned together due to their similar gene expression. We reflected this to varying extents in the structure of $\boldsymbol{\beta}^* \in \mathbb{R}^{p \times 12}$, where we consider $p \in \{250, 500, 1000, 2000\}$. We first randomly select 100 of the p rows to be nonzero in $\boldsymbol{\beta}^*$. Of these 100 rows, we select s many rows for which their coefficients are identical within the coarse groups described above, i.e. for these s rows, the coefficients for category A_1 and A_2 are identical, coefficients for category B_1 and B_2 are identical, and so on. For the remaining $100 - s$ nonzero rows of $\boldsymbol{\beta}^*$, the coefficients for all categories are unrelated. We sample each of the nonzero distinct elements from a Normal$(0, 2)$ distribution. This structure to $\boldsymbol{\beta}^*$ controls the similarity of fine cell types within a coarse label. With $s = 0$, even though

two categories may be binned together, they are unrelated and there is no true hierarchy of cell types. With larger s, fine categories within a coarse label are increasingly related, meaning there is true hierarchy to the cell type categories and cells are binned according to this hierarchy. We consider $s \in \{0, 20, 40, 60, 80\}$.

Finally, to simulate the effect of batch effects in the predictors, we generated $\boldsymbol{X}_{(k)} = \tilde{\boldsymbol{X}}_{(k)} + \boldsymbol{U}_{(k)}$ where $\boldsymbol{U}_{(k)} = (\boldsymbol{u}_{(k)1}, \ldots, \boldsymbol{u}_{(k)n_k})^\top \in \mathbb{R}^{n_k \times p}$. Each row of $\tilde{\boldsymbol{X}}_{(k)}$ is independently simulated from a p-dimensional multivariate normal distribution with mean 0 and AR(1) covariance matrix with lag 0.5. We consider a simple model for the batch effect itself, in which the batch effect is identical for every observation within a batch. This may also be reasonable in the real data, as the presence of background contamination, also known as ambient RNA, is a common source of batch effects, and it may affect all cells within the experiment similarly (after normalization) (Young and Behjati, 2020). Therefore, we generate $\boldsymbol{u}_{(k)} \in \mathbb{R}^p$ as a realization from a p-dimensional mean zero multivariate normal distribution with covariance $\boldsymbol{I}_p$ and set $\boldsymbol{U}_{(k)i,:} = a \cdot \boldsymbol{u}_{(k)}$, where a is a scalar chosen to control $b = \|\boldsymbol{U}_{(k)}\|_F / \|\tilde{\boldsymbol{X}}_{(k)}\|_F$. We consider $b \in \{0, 0.025, 0.05, 0.1, 0.2, 0.4\}$. The test dataset is observed with no batch effect, again in order to best evaluate parameter estimation.

5.2 Competing methods

We first consider two variants of our method, `IBMR-int` and `IBMR-NG`. For `IBMR-int`, we set $\boldsymbol{z}_{(k)i} = 1$ for all $i \in [n_k]$, $k \in [K]$, and fit the proposed model using (3). For `IBMR-NG`, we set $\boldsymbol{\gamma}_{(k)} = 0$ for all $k \in [K]$, where "NG" stands for "no Gamma", and estimate only $\boldsymbol{\alpha}^*$ and $\boldsymbol{\beta}^*$ using (3). This is a version of our method which ignores possible batches entirely.

We also consider two alternative methods, `subset` and `relabel`. For `subset`, we "mix-and-match" data from different datasets by subsetting each dataset to only the data that is annotated at the finest resolution and fit a model based on the stacked data. Specifically, define for $k \in [K]$, the set of indices in the kth dataset for which the outcome was observed at the finest resolution: $\mathcal{I}_k = \{i : |g_k(y_{(k)i})| = 1\}$. Then, we fit a group lasso-penalized multinomial logistic regression model using (3), but with $y_{(k)i}$ replaced with $g_k(y_{(k)i})$ for $k \in [K]$ and $i \in \mathcal{I}_k$, $\mathcal{C}_k$ replaced with $\mathcal{C}$ for $k \in [K]$, and $\mathcal{L}(\cdot, \cdot, \cdot)$ replaced with $-(\sum_{k=1}^K |\mathcal{I}_k|)^{-1} \sum_{k=1}^k \sum_{i \in \mathcal{I}_k} l_{(k)i}(\cdot, \cdot, \cdot)$. However, because of potential confounding, we do not consider a batch effect (i.e., require $\boldsymbol{\gamma}_{(k)} = \boldsymbol{0}$). The model can thus be fit using existing software (e.g., `glmnet`), but since the objective function is identical to our method when using only subsetted data, we use our implementation for consistency in the algorithm and convergence criterion.

For the other method, `relabel`, we first obtain estimates of $(\boldsymbol{\alpha}^*, \boldsymbol{\beta}^*)$ using `subset`, denoted $(\bar{\boldsymbol{\alpha}}^{\mathrm{S}}, \bar{\boldsymbol{\beta}}^{\mathrm{S}})$. Using these estimates, we can "relabel" our training data to have outcomes at the finest resolution by choosing the category with the highest conditional probability (as defined in (5)) $\tilde{y}^{\mathrm{S}}_{(k)i} = \arg\max_{l \in \mathcal{C}} [\tilde{\boldsymbol{C}}_{(k)}(\bar{\boldsymbol{\alpha}}^{\mathrm{S}}, \bar{\boldsymbol{\beta}}^{\mathrm{S}}, \mathbf{0})]_{i,l}$. We then fit the multinomial logistic regression model to $\tilde{y}^{\mathrm{S}}$, treating these as the observed labels. To be clear, all the training responses $\tilde{y}^{\mathrm{S}}$ are (synthetically) at the finest resolution, so one fits (3) but each $\mathcal{C}_k$ is replaced with $\mathcal{C}$.

Finally, we also consider oracle (`ORC`) versions of these methods, in which data at the finest resolution for all datasets is available. `IBMR-int-ORC` is the same as `IBMR-int`, with coarse resolution data replaced by the (otherwise unobserved) fine resolution data. By definition of `IBMR-NG`, `subset`, and `relabel`, when all the data is at the finest resolution, the estimators are equivalent to the standard group lasso penalized multinomial logistic regression model. Therefore, we name the oracle version of these estimators `GL-ORC`, where "GL" stands for "group lasso."

5.3 Results

We present the complete simulation study results in Figure 3. In the first column of Figure 3, we present results with the total sample size $N \in \{2400, 4800, 9600, 19200\}$ varying, and $p = 500$, $s = 40$, $b = 0.1$ fixed. We see that with increasing sample size, the KL divergence, Hellinger distance, and error rates decrease for all methods, as expected. Of the non-oracle methods, for all sample sizes considered, `IBMR-int` and `IBMR-NG` perform the best and are much closer to the oracle methods in which all data is observed at the finest resolution, as compared to `relabel` and `subset`.

In the second column of Figure 3, we vary the total number of genes $p \in \{250, 500, 1000, 2000\}$ (all with 100 nonzero rows of $\boldsymbol{\beta}^*$), with $N = 4800$, $s = 40$, and $b = 0.1$ fixed. We see that with increasing number of genes, all performance metrics increase for all methods, as expected. Again, the `IBMR`-based methods are much closer to the oracle methods than `relabel` and especially `subset`.

In the third column of Figure 3, we vary the similarity of cell type categories within coarser groups by considering $s \in \{0, 20, 40, 60, 80\}$, the number of nonzero rows of $\boldsymbol{\beta}^*$ for which fine categories within a coarse label share coefficients. We fix $N = 4800$, $p = 500$, and $b = 0.1$. With s increasing, fine categories within a coarse group become more similar, thus the Hellinger distance and error rates increase for all methods. This is because larger s makes it more difficult to distinguish between the fine categories within a coarse group. KL

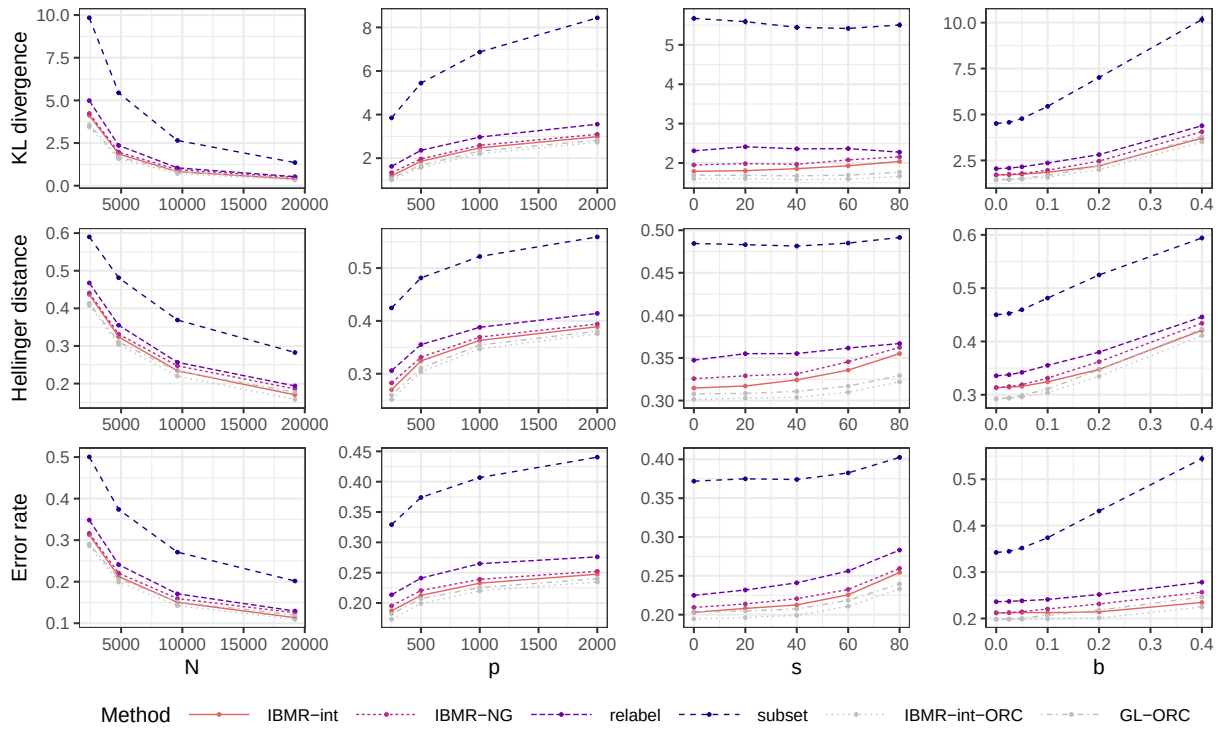

Figure 3: (top) Kullback-Leibler divergence, (middle) Hellinger distance, and (bottom) error rate for six competing methods with varying (left) N, the total sample size; (middle left) p, the total number of features; (middle right) s, the number of nonzero features which have shared coefficients for fine categories within a coarse label; and (right) b, the ratio of the norm of the batch effect and norm of the true predictors. Error bars denote the standard error for each method across 50 replicates. Throughout, the defaults are $N = 4800$, $p = 500$, $s = 40$, $b = 0.1$.

divergence is relatively constant, but slightly increases for `IBMR`-based methods at s increases. For all values of s, `IBMR`-based methods again perform more similar to the oracle methods than do `relabel` and `subset`.

For simulation results displayed in the last (rightmost) column of Figure 3, we fixed $N = 4800$, $p = 500$, and $s = 40$ and varied the batch effect size by considering $b \in \{0, 0.025, 0.05, 0.1, 0.2, 0.4\}$. We see that with increasing batch effect, `IBMR-int` outperforms `IBMR-NG`, with the error rate of `IBMR-int` staying relatively constant until $b = 0.2$. Of course $b = 0.2$ represents a quite large batch effect: in this situation the norm of the batch effect is, loosely speaking, 20 percent of the norm of the true gene expression. Again, `IBMR`-based methods are closest to oracle methods.

6 Application to integrative cell type annotation

In this section, we apply our method to single-cell gene expression data from 10 publicly available peripheral blood mononuclear cells (PBMC) datasets with annotations at various resolutions and labels across datasets. These datasets can be downloaded in a standardized format as `Bioconductor SingleCellExperiment` objects from `https://github.com/keshav-motwani/AnnotatedPBMC`. Table 1 lists the datasets used and the number of cell type labels per dataset. Table 3 gives the specific labels used in each dataset. The specifics of preprocessing of the data are described in Section A of the Supplementary Material.

6.1 Comparison to `subset` and `relabel`

In order to assess the performance of our method compared to competitors, we fit each method on eight datasets at a time, leaving out one validation dataset and one test dataset. In order to keep the binning functions the same across all train/validation/test splits, we kept the `hao_2020` dataset in the training set always because it had the finest resolution labels. We therefore defined the finest resolution categories across all datasets ($\mathcal{C}$) to be those used in the `hao_2020` dataset, and defined the binning functions (f_k) as graphically depicted in Figure 2. We evaluate performance over all 72 combinations of training/validation/test splits of eight training datasets (necessarily containing `hao_2020`), one validation dataset and one test dataset. We choose tuning parameters based on validation set negative log-likelihood, and measure performance using test set negative log-likelihood and error rate with the fitted parameters.

To reduce computational complexity, we perform screening on genes by ranking genes as described in Section A of the Supplementary Material, and select the first p genes for each dataset. Also, for each training dataset, we sample n_k cells using a weighted sampling procedure – also described in Section A of the Supplementary Material – in order to encourage oversampling extremely rare cell types and undersampling common cell types.

We first assessed the test set negative log-likelihood of each of the non-oracle methods considered in the simulation study when varying the sample size per dataset $n_k \in \{1250, 2500, 5000, 10000\}$ with the number of genes $p = 1000$ fixed. We repeat this five times, as the sampling of cells from each dataset is random. We then compute the negative log-likelihood for nine test datasets, each using one of the remaining eight datasets as a validation set, and the rest of the datasets as traning datasets, across five replicates. We first compute the average and standard error of the negative log likleihood across the five

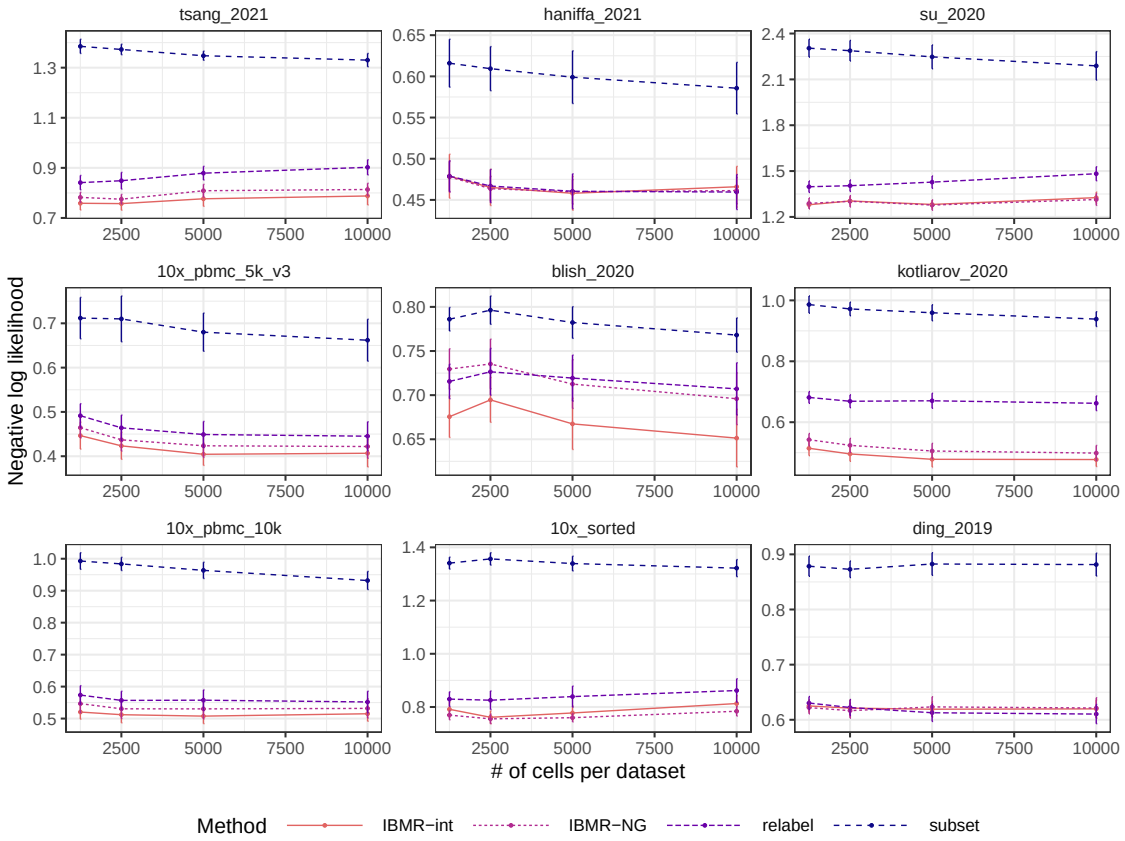

Figure 4: Negative log-likelihood for each method considered, for each test dataset (subplots), for varying numbers of cells per dataset used for fitting the model with the number of genes $p = 1000$ fixed. Points denote the average of the average negative log-likelihood across validation sets, for which each training/validation/test dataset combination had five replicates of different subsampled training datasets, and error bars show the standard error of averages across validation sets.

replicates for each train/validation/test dataset combination, and then summarize the results for each test dataset by taking the average and standard error of these averages across all of the train/validation dataset combinations considered. These summarized results per test dataset are shown in Figures 4, with the complete results for each validation and test dataset combination in Figure B.2 of the Supplementary Material. In general, the negative log-likelihood decreases or stays relatively constant with increasing sample size for all methods. `IBMR-int` tends to perform slightly better than `IBMR-NG` on some datasets, as fitting a batch-specific intercept term helps in these cases. In general, `IBMR`-based methods always do as well or better than `relabel`, and `subset` always performs the poorest.

While the negative log-likelihood illustrates prediction performance in terms of estimated

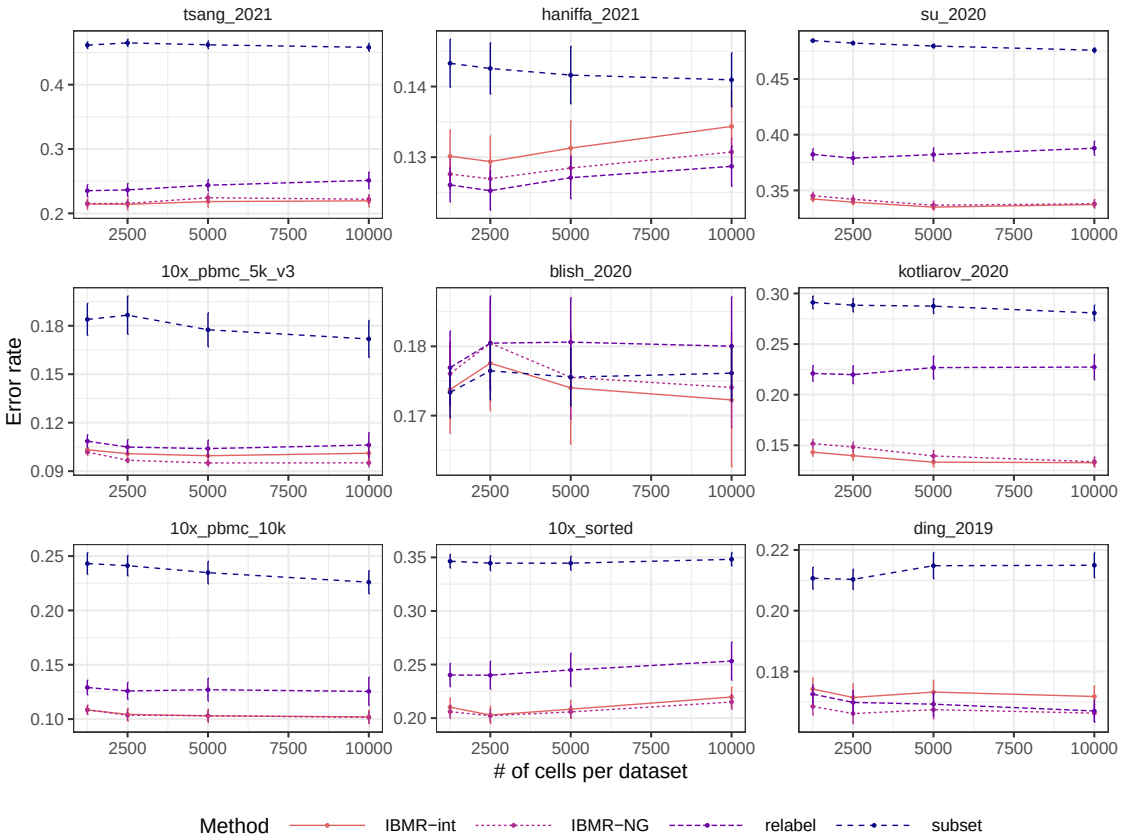

Figure 5: Error rate for each method considered, for each test dataset (subplots), for varying numbers of cells per dataset used for fitting the model with the number of genes $p = 1000$ fixed. Points denote the average of the average negative log-likelihood across validation sets, for which each training/validation/test dataset combination had five replicates of different subsampled training datasets, and error bars show the standard error of averages across validation sets.

probabilities as a continuous value, it is more difficult to interpret than, say, classification error rate. For this reason, we also considered error rate, which is slightly more complicated to define in this setting. Specifically, in order to define an "error," we must make predictions from the same set of labels used in the test dataset. We refer to these as "coarse predictions" and define them as follows. Let $f_{\text{test}} : \mathcal{C} \to \mathcal{C}_{\text{test}}$ be the binning function for the test dataset labels, and $g_{\text{test}} = f_{\text{test}}^{-1}$ be the unbinning function as defined before. Because there may be labels in $\mathcal{C}_{\text{test}}$ which are bins of categories in $\mathcal{C}$ not observed in the test dataset in order to properly define the binning functions (named "unobserved" for example, as described earlier), we define $\ddot{\mathcal{C}}_{\text{test}}$ as follows: $\ddot{\mathcal{C}}_{\text{test}} = \{j \in \mathcal{C}_{\text{test}} : \sum_{i=1}^{n_{\text{test}}} \mathbb{1}\left(y_{(\text{test})i} = j\right) > 0\}$. That is, it is a subset of $\mathcal{C}_{\text{test}}$ for which we actually observe cells annotated with that label.

We can then predict only within these labels to be consistent with the observed labels, which we call "coarse predictions". We have that the predicted probabilities at this coarse level are defined by

$$[\hat{\boldsymbol{P}}_{(\text{test})}]_{i,j} = \frac{\sum_{l \in g_{\text{test}}(j)} \exp(\hat{\boldsymbol{\alpha}}_l + \boldsymbol{x}_{(\text{test})i}^\top \hat{\boldsymbol{\beta}}_l)}{\sum_{u \in \ddot{\mathcal{C}}_{\text{test}}} \sum_{v \in g_{\text{test}}(j)} \exp(\hat{\boldsymbol{\alpha}}_v + \boldsymbol{x}_{(\text{test})i}^\top \hat{\boldsymbol{\beta}}_v)}, \quad j \in \ddot{\mathcal{C}}_{\text{test}},$$

and we then define the ith "coarse prediction" as $\arg\max_{j \in \ddot{\mathcal{C}}_{(\text{test})}} \{[\hat{\boldsymbol{P}}_{(\text{test})}]_{i,j}\}$.

The summarized error rate results per test dataset are shown in Figure 5 and complete results in Figure B.2 of the Supplementary Material. In general, there is increased variability in results across test datasets for error rate than for negative log-likelihood. Even so, in six out of nine test datasets considered, `IBMR-int` and `IBMR-NG` outperform `relabel` and `subset`, with `subset` resulting in error rates nearly double those of `IBMR-int`, `IBMR-NG`, and `relabel` in some cases.

We next performed a similar experiment: with the sample size per dataset $n_k = 5000$ fixed, we varied the number of predictors $p \in \{250, 500, 1000, 2000\}$. Once again, we adopted the same setup for training/validation/test splits, and 5 replicates per split to account for subsampling variability. The summarized results per test dataset are shown in the Supplementary Material, in Figures B.4 (negative log-likelihood) and B.5 (error rate), with the complete results for each validation and test dataset combination in Figures B.6 (negative log-likelihood) and B.7 (error rate). Overall, we see that accounting for the batch effect with `IBMR-int` usually improves upon `IBMR-NG`, with `relabel` generally falling behind `IBMR`-based methods. The method `subset` consistently performs poorly compared to the other methods for all datasets.

6.2 Annotating or refining cell type labels on new datasets

In this section, we use our fitted model to annotate and refine cell type labels on a new dataset. For this, we turn our attention to the `IBMR-int` model fit in the last section with `tsang_2021` as the validation set and `ding_2019` as the test dataset, for the first replicate of the experiment with $n_k = 10000$ and $p = 1000$. We choose `tsang_2021` to be the validation set because it has the finest annotations over all validation sets considered and we chose to predict on `ding_2019` because it has the most coarse annotations.

There are three types of predictions we may consider: (i) a prediction of the finest resolution categories based on our model, which was the primary motivation; (ii) if we have

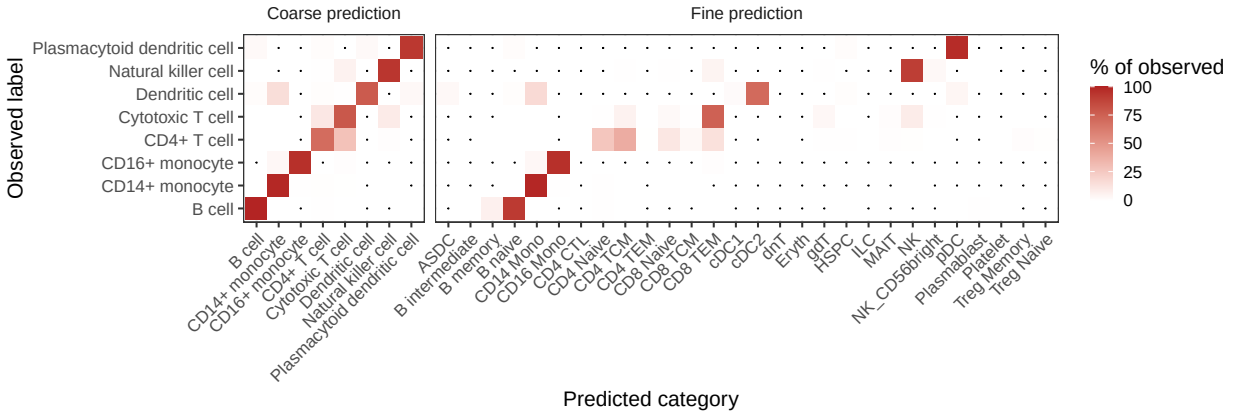

Figure 6: Heatmap showing the percentage of cells in (left) coarse and (right) fine predicted categories for each observed label in the `ding_2019` dataset. Dots indicate that exactly 0 cells are in that combination of observed label and prediction.

already observed coarse annotations on a dataset, we can make predictions of the finest resolution categories, conditional on already observed coarse label; or (iii) coarse predictions as described in the previous section for performance evaluation. Note that (ii) is especially useful when only coarse labels are used in annotating a dataset initially, but more refined annotations are desired for downstream analyses.

In the case where we are simply interested in predicting fine resolution categories on a dataset with only gene expression observed, (i), we define the ith "fine prediction" as $\arg\max_{l \in \mathcal{C}}\{[\tilde{\boldsymbol{P}}_{(\text{test})}(\hat{\boldsymbol{\alpha}}, \hat{\boldsymbol{\beta}}, \mathbf{0})]_{i,l}\}$ where $\tilde{\boldsymbol{P}}_{(\text{test})}$ is defined as in (4). Alternatively, if we want to predict fine resolution categories, but have observed both gene expression and coarse resolution annotations, we can condition on the coarse label and obtain conditional predictions, i.e., prediction of type (ii). In effect, this refines the existing annotations based on the fitted model and provides more detailed annotations. In this case, we define the "conditional predictions" as $\arg\max_{l \in \mathcal{C}}\{[\tilde{\boldsymbol{C}}_{(\text{test})}(\hat{\boldsymbol{\alpha}}, \hat{\boldsymbol{\beta}}, \mathbf{0})]_{i,l}\}$ where $\tilde{\boldsymbol{C}}_{(\text{test})}$ is defined as in (5). Note that if an observation already has a fine label, then the label will not change by the definition of the conditional probabilities, so there will not be contradictory results.

In Figure 6, we show the coarse predictions and fine predictions, and the percentage of each of the observed labels which are predicted as a given category for these two types of predictions. The model does very well at predicting at the coarse level, with few predictions in the off-diagonal elements of the heatmap. The fine predictions generally agree very well with the coarse observed annotations, while giving additional information. In Figure 7, we once again show the same coarse predictions as a reference, and also take advantage of the already coarsely labeled data to provide predictions conditional on the observed coarse an-

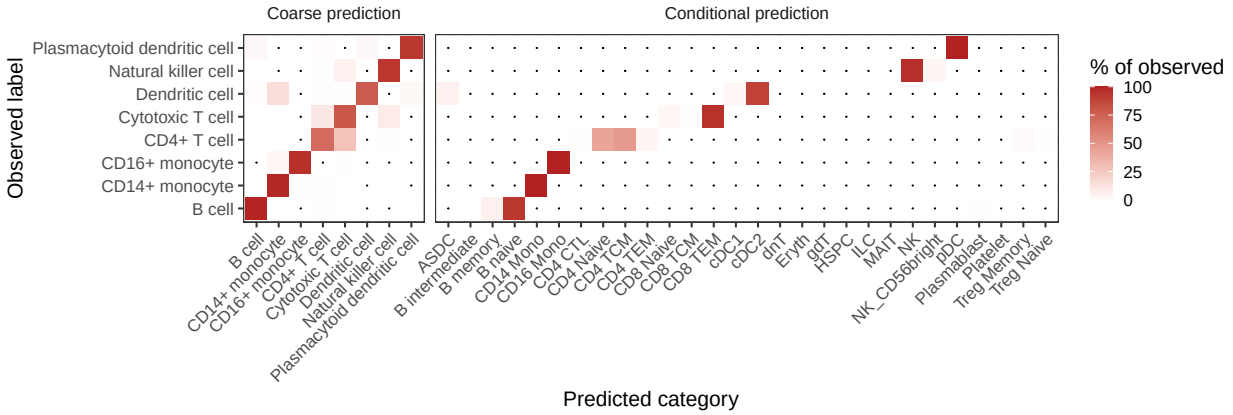

Figure 7: Heatmap showing the percentage of cells in (left) coarse and (right) conditional predicted categories for each observed label in the `ding_2019` dataset. Dots indicate that exactly 0 cells are in that combination of observed label and prediction. Note that the difference between Figure 6 and this figure is that the (right) panel is showing conditional predictions rather than fine predictions.

notations. These conditional predictions only split up an observed label into finer categories by definition, so they provide additional detail and do not ever contradict the initial coarse annotations.

In order to showcase interpretability of the model coefficients for this same fitted model considered above, we display the genes corresponding to the top 10 standardized coefficients per finest resolution category in Table 2. Many of these genes overlap with commonly used marker genes for these cell types, as shown in bold in 2, based on marker genes by Hao et al. (2020) for these categories. Note that these marker genes were defined by Hao et al. (2020) only on the `hao_2020` dataset, and were the result of performing hypothesis testing on the gene expression of a particular gene within cells of a category compared to all other cells, so these same genes may not be optimal for classification purposes.

7 Discussion

In this article, we proposed a new method for integrating multiple datasets where observation labels are available at different resolutions. Overall, `IBMR`-based methods outperformed other competitors under all simulation settings, and generally performed better in the application to single-cell genomics data, with `relabel` only having close performance in a small number of cases. However, there are additional aspects of the methods to be considered in terms of performance and practical usage. Specifically, while `relabel` could be considered a two-

Cell type	Genes									
ASDC	TCF4	SOX4	**PPP1R14A**	HLA-DRA	GPR183	S100A4	IRF8	CD74	ITM2C	S100A10
B intermediate	**MS4A1**	**CD79A**	**BANK1**	**RALGPS2**	GPR183	HLA-DRA	TCF4	MALAT1	**TNFRSF13B**	TNFRSF13C
B memory	**MS4A1**	HLA-DRA	**BANK1**	LTB	**CD79A**	ITGB1	TNFRSF13B	CD74	MALAT1	**TNFRSF13C**
B naive	**MS4A1**	**CD79A**	CD74	HLA-DRA	**TCL1A**	LTB	FCGR3A	BANK1	LINC00926	**YBX3**
CD14 Mono	**LYZ**	**S100A8**	TYROBP	HLA-DRA	**FCN1**	**CD14**	FTL	PSAP	AIF1	HLA-DRB1
CD16 Mono	**FCGR3A**	**AIF1**	**MS4A7**	**LST1**	**CDKN1C**	TYROBP	PSAP	NAP1L1	S100A4	**IFITM3**
CD4 CTL	CCL5	**GNLY**	IL7R	**NKG7**	S100A4	**ITGB1**	CD3G	**IL32**	MALAT1	CD3D
CD4 Naive	LTB	**CCR7**	CD3D	MALAT1	CD3E	**NOSIP**	CD7	NKG7	**FHIT**	**LDHB**
CD4 TCM	S100A4	CD3D	**LTB**	**IL7R**	CD52	ANXA1	**ITGB1**	**IL32**	S100A11	CD40LG
CD4 TEM	**IL7R**	**GZMK**	**CCL5**	**KLRB1**	**IL32**	**LTB**	GPR183	CD3G	S100A4	MALAT1
CD8 Naive	**CD8B**	**CD8A**	CTSW	CD3D	**S100B**	MALAT1	FCGR3A	AIF1	CD7	HCST
CD8 TCM	**CD8B**	**CD8A**	**IL7R**	CCL5	IL32	LTB	S100A4	ITGB1	**ANXA1**	CTSW
CD8 TEM	**CCL5**	**CD8A**	**CD8B**	**GZMK**	**NKG7**	CD3D	CTSW	IL32	MALAT1	**GZMH**
cDC1	HLA-DRA	**CADM1**	CD74	IRF8	HLA-DPB1	HLA-DPA1	LYZ	ID2	S100A10	HLA-DRB1
cDC2	CD74	**FCER1A**	HLA-DRA	**CD1C**	HLA-DPA1	TYROBP	HLA-DPB1	VIM	S100A10	CST3
dnT	**GZMK**	**NUCB2**	GPR183	CD8B	MALAT1	CD3D	CD3G	HBB	**FXYD2**	CCR7
Eryth	HBB	CD8B	CD8A	FCGR3A	IL7R	MS4A1	AHNAK	PSAP	DUSP1	TNFAIP3
gdT	CCL5	IL7R	**KLRD1**	CD3D	**KLRC1**	IL32	CD3G	KLRB1	**NKG7**	RTKN2
HSPC	**SPINK2**	**PRSS57**	SOX4	AIF1	RPS20	HLA-DRA	**CYTL1**	PPBP	CD79A	LST1
ILC	**KLRB1**	IL7R	ITGB1	**TNFRSF18**	GPR183	**TNFRSF4**	LTB	IL2RA	MALAT1	SPINK2
MAIT	**KLRB1**	**GZMK**	**IL7R**	CD8A	CD8B	CCL5	S100A4	LTB	**NKG7**	**NCR3**
NK	**GNLY**	FCGR3A	**TYROBP**	**PRF1**	CTSW	**NKG7**	KLRB1	KLRD1	**KLRF1**	CD247
NK˙CD56bright	GNLY	GZMK	**XCL1**	CTSW	**KLRC1**	KLRD1	TYROBP	KLRB1	**XCL2**	NKG7
pDC	TCF4	**ITM2C**	**MZB1**	**SERPINF1**	CD74	IRF8	**PLD4**	HLA-DRA	TCL1A	GPR183
Plasmablast	**MZB1**	CD79A	ITM2C	ITGB1	**TNFRSF13B**	PRDM1	**CPNE5**	AQP3	**POU2AF1**	TCF4
Platelet	**PPBP**	**TUBB1**	CD8B	SPARC	**NRGN**	HBB	CCL5	IL7R	CD8A	ITGB1
Treg Memory	**RTKN2**	IL32	**TIGIT**	**CTLA4**	**FOXP3**	**S100A4**	**IKZF2**	IL2RA	ITGB1	LTB
Treg Naive	IL32	**RTKN2**	CD3D	CD3E	**IL2RA**	LTB	**FOXP3**	DUSP1	CTLA4	IKZF2

Table 2: Top 10 genes with largest standardized coefficients for each of the finest resolution categories (rows). These genes align with commonly used marker genes (bolded) for manually annotating cell types based on Hao et al. (2020).

step "approximation" to `IBMR-NG`, it involves two tuning parameters, and for each tuning parameter combination, two optimization problems must be solved. Each of these problems are similar in complexity to `IBMR-NG`. Therefore, `IBMR-NG`, which only involves one tuning parameter and one optimization problem, is arguably preferable to `relabel` as it is faster and, in general, more accurately estimates test set probabilities. Additionally, in the real data and even under large batch effects in simulations, `IBMR-NG` performs similarly to `IBMR-int`, which also involves two tuning parameters. Therefore, it may be reasonable to use `IBMR-NG` as an approximation to `IBMR-int` to further reduce computing times. These latter findings cohere with those in Ma et al. (2021), who found adjusting for batch effects did not have a substantial impact on cell type prediction.

There are multiple directions for future research. First, we have assumed a multinomial logistic regression model. Instead, it may be preferable to use a semiparametric or non-parameteric approach for modeling the probabilities (2). For example, the application of random forests to this context may perform well. Second, our method did not exploit the similarity of cell types within a coarse category in any way. For example, in Section 5 we generated data such that coefficient vectors for two cell types belonging to a coarse category were more similar compared to cell types which did not belong to a shared coarse category. We are currently developing an extension of our method which can exploit this feature.

Acknowledgements

Keshav Motwani's research was supported by the Goldwater Foundation as well as the University Scholars Program at the University of Florida. Aaron J. Molstad's research was supported by National Science Foundation grant DMS-2113589.

References

10x Genomics (2018). 10k PBMCs from a healthy donor - gene expression and cell surface protein. `https://support.10xgenomics.com/single-cell-gene-expression/datasets/3.0.0/pbmc_10k_protein_v3`.

10x Genomics (2019). 5k Peripheral blood mononuclear cells (PBMCs) from a healthy donor with cell surface proteins (v3 chemistry). `https://support.10xgenomics.com/single-cell-gene-expression/datasets/3.0.2/5k_pbmc_protein_v3`.

Abdelaal, T., Michielsen, L., Cats, D., Hoogduin, D., Mei, H., Reinders, M. J., and Mahfouz, A. (2019). A comparison of automatic cell identification methods for single-cell RNA sequencing data. *Genome Biology*, 20(1):194.

Amezquita, R. A., Lun, A. T., Becht, E., Carey, V. J., Carpp, L. N., Geistlinger, L., Marini, F., Rue-Albrecht, K., Risso, D., and Soneson, C. (2020). Orchestrating single-cell analysis with bioconductor. *Nature Methods*, 17(2):137–145.

Conde, C. D., Gomes, T., Jarvis, L. B., Xu, C., Howlett, S., Rainbow, D., Suchanek, O., King, H., Mamanova, L., and Polanski, K. (2021). Cross-tissue immune cell analysis reveals tissue-specific adaptations and clonal architecture across the human body. *bioRxiv*.

Ding, J., Adiconis, X., Simmons, S. K., Kowalczyk, M. S., Hession, C. C., Marjanovic, N. D., Hughes, T. K., Wadsworth, M. H., Burks, T., and Nguyen, L. T. (2019). Systematic comparative analysis of single cell rna-sequencing methods. *BioRxiv*, page 632216.

Haghverdi, L., Lun, A. T., Morgan, M. D., and Marioni, J. C. (2018). Batch effects in single-cell RNA-sequencing data are corrected by matching mutual nearest neighbors. *Nature Biotechnology*, 36(5):421–427.

Hao, Y., Hao, S., Andersen-Nissen, E., Mauck, W. M., Zheng, S., Butler, A., Lee, M. J., Wilk, A. J., Darby, C., and Zagar, M. (2020). Integrated analysis of multimodal single-cell data. *bioRxiv*.

Hie, B., Bryson, B., and Berger, B. (2019). Efficient integration of heterogeneous single-cell transcriptomes using Scanorama. *Nature Biotechnology*, 37(6):685–691.

Huang, Y., Zhang, Q., Zhang, S., Huang, J., and Ma, S. (2017). Promoting similarity of sparsity structures in integrative analysis with penalization. *Journal of the American Statistical Association*, 112(517):342–350.

Korsunsky, I., Millard, N., Fan, J., Slowikowski, K., Zhang, F., Wei, K., Baglaenko, Y., Brenner, M., Loh, P.-r., and Raychaudhuri, S. (2019). Fast, sensitive and accurate integration of single-cell data with Harmony. *Nature Methods*, 16(12):1289–1296.

Kotliarov, Y., Sparks, R., Martins, A. J., Mulè, M. P., Lu, Y., Goswami, M., Kardava, L., Banchereau, R., Pascual, V., and Biancotto, A. (2020). Broad immune activation underlies shared set point signatures for vaccine responsiveness in healthy individuals and disease activity in patients with lupus. *Nature Medicine*, 26(4):618–629.

Lange, K. (2016). *MM optimization algorithms*. SIAM.

Liu, C., Martins, A. J., Lau, W. W., Rachmaninoff, N., Chen, J., Imberti, L., Mostaghimi, D., Fink, D. L., Burbelo, P. D., and Dobbs, K. (2021). Time-resolved systems immunology reveals a late juncture linked to fatal COVID-19. *Cell*, 184(7):1836–1857.

Ma, W., Su, K., and Wu, H. (2021). Evaluation of some aspects in supervised cell type identification for single-cell RNA-seq: classifier, feature selection, and reference construction. *Genome Biology*, 22(1):1–23.

Molstad, A. J. and Patra, R. K. (2021). Dimension reduction for integrative survival analysis. *arXiv preprint arXiv:2108.02143*.

Molstad, A. J. and Rothman, A. J. (2021). A likelihood-based approach for multivariate categorical response regression in high dimensions. *Journal of the American Statistical Association*.

Obozinski, G., Wainwright, M. J., and Jordan, M. I. (2011). Support union recovery in high-dimensional multivariate regression. *The Annals of Statistics*, 39(1):1–47.

Parikh, N. and Boyd, S. (2014). Proximal algorithms. *Foundations and Trends in Optimization*, 1(3):127–239.

Pasquini, G., Rojo Arias, J. E., Schäfer, P., and Busskamp, V. (2021). Automated methods for cell type annotation on scRNA-seq data. *Computational and Structural Biotechnology Journal*, 19:961–969.

Polson, N. G., Scott, J. G., and Willard, B. T. (2015). Proximal algorithms in statistics and machine learning. *Statistical Science*, 30(4):559–581.

Schaum, N., Karkanias, J., Neff, N. F., May, A. P., Quake, S. R., Wyss-Coray, T., Darmanis, S., Batson, J., Botvinnik, O., and Chen, M. B. (2018). Single-cell transcriptomics of 20 mouse organs creates a tabula muris: The tabula muris consortium. *Nature*, 562(7727):367.

Shasha, C., Tian, Y., Mair, F., Miller, H. E., and Gottardo, R. (2021). Superscan: Supervised single-cell annotation. *bioRxiv*.

Simon, N., Friedman, J., Hastie, T., and Tibshirani, R. (2013). A sparse-group lasso. *Journal of Computational and Graphical Statistics*, 22(2):231–245.

Stephenson, E., Reynolds, G., Botting, R. A., Calero-Nieto, F. J., Morgan, M. D., Tuong, Z. K., Bach, K., Sungnak, W., Worlock, K. B., and Yoshida, M. (2021). Single-cell multi-omics analysis of the immune response in COVID-19. *Nature Medicine*, 27(5):904–916.

Su, Y., Chen, D., Yuan, D., Lausted, C., Choi, J., Dai, C. L., Voillet, V., Duvvuri, V. R., Scherler, K., and Troisch, P. (2020). Multi-omics resolves a sharp disease-state shift between mild and moderate COVID-19. *Cell*, 183(6):1479–1495.

Ventz, S., Mazumder, R., and Trippa, L. (2021). Integration of survival data from multiple studies. *Biometrics*.

Wilk, A. J., Rustagi, A., Zhao, N. Q., Roque, J., Martínez-Colón, G. J., McKechnie, J. L., Ivison, G. T., Ranganath, T., Vergara, R., and Hollis, T. (2020). A single-cell atlas of the peripheral immune response in patients with severe COVID-19. *Nature Medicine*, 26(7):1070–1076.

Wolf, F. A., Angerer, P., and Theis, F. J. (2018). Scanpy: large-scale single-cell gene expression data analysis. *Genome Biology*, 19(1):1–5.

Xu, Y. and Yin, W. (2017). A globally convergent algorithm for nonconvex optimization based on block coordinate update. *Journal of Scientific Computing*, 72(2):700–734.

Young, M. D. and Behjati, S. (2020). SoupX removes ambient RNA contamination from droplet-based single-cell RNA sequencing data. *GigaScience*, 9(12). giaa151.

Yuan, M. and Lin, Y. (2006). Model selection and estimation in regression with grouped variables. *Journal of the Royal Statistical Society: Series B (Statistical Methodology)*, 68(1):49–67.

Zhao, Q., Shi, X., Huang, J., Liu, J., Li, Y., and Ma, S. (2015). Integrative analysis of '-omics' data using penalty functions. *Wiley Interdisciplinary Reviews: Computational Statistics*, 7(1):99–108.

Zheng, G. X., Terry, J. M., Belgrader, P., Ryvkin, P., Bent, Z. W., Wilson, R., Ziraldo, S. B., Wheeler, T. D., McDermott, G. P., and Zhu, J. (2017). Massively parallel digital transcriptional profiling of single cells. *Nature Communications*, 8(1):1–12.